ELSEVIER

Chemical Geology 173 (2001) 3–30

CHEMICAL GEOLOGY
INCLUDING
ISOTOPE GEOSCIENCE

www.elsevier.com/locate/chemgeo

Fluid inclusion gas compositions from an active magmatic–hydrothermal system: a case study of The Geysers geothermal field, USA

Joseph N. Moore [a,*], David I. Norman [b], B. Mack Kennedy [c]

[a] *Energy & Geoscience Institute, University of Utah, Salt Lake City, UT 84108, USA*
[b] *Department of Earth and Environmental Science, New Mexico Institute of Mining and Technology, Socorro, NM 87801, USA*
[c] *Center for Isotope Geochemistry, E.O. Lawrence Berkeley National Laboratory, Berkeley, CA 94720, USA*

Accepted 18 January 2000

Abstract

Hydrothermal alteration and the active vapor-dominated geothermal system at The Geysers, CA are related to a composite hypabyssal granitic pluton emplaced beneath the field 1.1 to 1.2 million years ago. Deep drill holes provide a complete transect across the thermal system and samples of the modern-day steam. The hydrothermal system was liquid-dominated prior to formation of the modern vapor-dominated regime at 0.25 to 0.28 Ma. Maximum temperatures and salinities ranged from 440°C and 44 wt.% NaCl equivalent in the biotite hornfels adjacent to the pluton to 305°C and 5 wt.% NaCl equivalent at distances of 1730 m from the intrusive contact. The major, minor, and noble gas compositions of fluid inclusions in the hydrothermally altered rocks were integrated with microthermometric and mineralogic data to determine their sources and the effects of mixing and boiling. Major and minor gaseous species were released from the inclusions by crushing or thermal decrepitation; noble gases were released by crushing. The samples were analyzed by mass spectrometry. The analyses document the presence of magmatic, crustal, and meteoric components in the trapped fluids. Hydrothermal fluids present during the liquid-dominated phase of the system contained gaseous species derived mainly from crustal and magmatic sources. At The Geysers, N_2/Ar ratios greater than 525 and $^3He/^4He$ ratios of 6–10.7 Ra are diagnostic of a magmatic component. Crustal gas has CO_2/CH_4 ratios less than 4, N_2/Ar ratios between 45 and 525, and low $^3He/^4He$ ratios (0.5 Ra). Meteoric fluids have CO_2/CH_4 ratios greater than 4 and N_2/Ar ratios between 38 (air-saturated water) and 84 (air). However, N_2/Ar ratios between 15 and 110 can result from boiling. Ratios less than 15 reflect the incorporation of N_2 into NH_3-bearing clay minerals. In the central Geysers, the incursion of meteoric fluids occurred during the transition from the liquid- to vapor-dominated regime. Variations in the relative CH_4, CO_2, and H_2 contents of the gas analyses demonstrate that boiling took place under open-system conditions. The gas data indicate that the inclusions have remained closed to the diffusion of He and H_2 since their formation. © 2001 Elsevier Science B.V. All rights reserved.

Keywords: Fluid inclusions; Gas analysis; The Geysers; Geothermal; Vapor-dominated; Noble gases; Crustal gas; Magmatic gas; Meteoric gas

* Corresponding author.

0009-2541/01/$ - see front matter © 2001 Elsevier Science B.V. All rights reserved.
PII: S0009-2541(00)00265-5

1. Introduction

The Geysers is the largest of the world's productive geothermal systems and one of the few that are vapor-dominated and yield only dry steam. Since the 1960s, more than 705 deep wells have been drilled, providing a complete transect from the underlying pluton that triggered hydrothermal activity to the outer portions of the thermal aureole it created. Previous petrologic studies of The Geysers have defined the mineral parageneses, whole-rock oxygen isotope distributions, and fluid inclusion salinities and temperatures within the alteration halo and the plutonic rocks (e.g., Sternfeld, 1989; Hulen et al.,1992; Lambert and Epstein, 1992; Hulen and Walters, 1993; Moore and Gunderson, 1995; Moore et al., 1998a). These investigations have yielded an unusually comprehensive record of the system's history from its inception as a liquid-dominated hydrothermal system 1.1 to 1.2 million years ago to the initial development of the present vapor-dominated regime at 0.28 to 0.25 Ma (Hulen et al., 1997; Dalrymple et al., 1999). Although fluid inclusion temperatures and salinities suggest trapping of magmatic, crustal (connate or metamorphic), and meteoric fluids (Moore and Gunderson, 1995), positive identification of the fluid sources and the relative contributions of these fluids in time and space could not be established. In this paper, we expand on earlier studies of The Geysers and utilize the gas compositions of fluid inclusions to help trace the sources of the fluids, their chemistries, and the processes that have affected them.

2. Geologic setting

2.1. Overview of geologic relationships

The Geysers is located 150 km north of San Francisco, on the southwestern edge of the Pliocene to Holocene Clear Lake volcanic field (Fig. 1; Donnelly-Nolen et al., 1993). Here, hydrothermal activity is related to a composite hypabyssal granitic intrusion that reaches to within 0.7 km of the surface. The pluton consists of three major phases that together have a volume exceeding 100 km^3 (Fig. 2; Donnelly-Nolan et al., 1993; Hulen and Walters, 1993; Hulen and Nielson,1996). The oldest phases include an orthopyroxene–biotite granite and a biotite–microgranite that appear to be cogenetic. The youngest phase is a hornblende-biotite-orthopyroxene granodiorite. Recent UP-b zircon ages and $^{40}Ar/^{39}Ar$ spectrum dating (Dalrymple et al., 1999) indicate that the pluton was emplaced between 1.13 ± 0.06 and 1.23 ± 0.07 Ma. Intrusive activity has continued, at least intermittently, during the last 1 Ma. At 0.57 Ma, rhyolite dikes were emplaced in the southeastern Geysers (Pulka, 1991). The deposition of adularia at the same time in the central part of the field may be a further reflection of this event (Hulen et al., 1997). Measured temperatures of up to 342°C (Walters et al., 1988) in the northwest Geysers and steam with $^3He/^4He$ ratios of 6.6 to 8.3 Ra (Kennedy and Truesdell, 1996) provide evidence of still younger intrusive activity. Although the influence of this intrusion on the modern geothermal system is most evident in the northwest, high R/Ra values in steam from the central and southeast Geysers (Torgersen and Jenkins, 1982) suggest that it's influence may extend underneath much of the geothermal field but is buffered by deep meteoric recharge from the southeast (Kennedy and Truesdell, 1996). This intrusive activity appears to be part of a northeast-trending belt of recent magmatism (Walters et al., 1996) that is associated with high-temperature geothermal activity within the Clear Lake volcanic field (i.e., on the flanks of Mt. Hanna and at the Sulphur Bank Mine; Fig. 1).

The Geysers pluton was emplaced within deep oceanic deposits of the Jurassic to Cretaceous Franciscan Complex (McLaughlin, 1981). At The Geysers, this lithologically diverse formation is dominated by metagraywacke, which contains the bulk of the steam being produced. However, significant thicknesses of argillite, chert, greenstone, serpentinite, and exotic blocks metamorphosed up to the blueschist facies are also present. Lateral and vertical variations in both metamorphic grade and lithology, which can be related to northeast-directed subduction and imbricate thrusting during Mesozoic to Early Tertiary time (McNitt, 1968; McLaughlin, 1981, Thompson, 1989), are characteristic of the Franciscan Complex. Superimposed on this early tectonic regime are north- to northwest-trending strike–slip

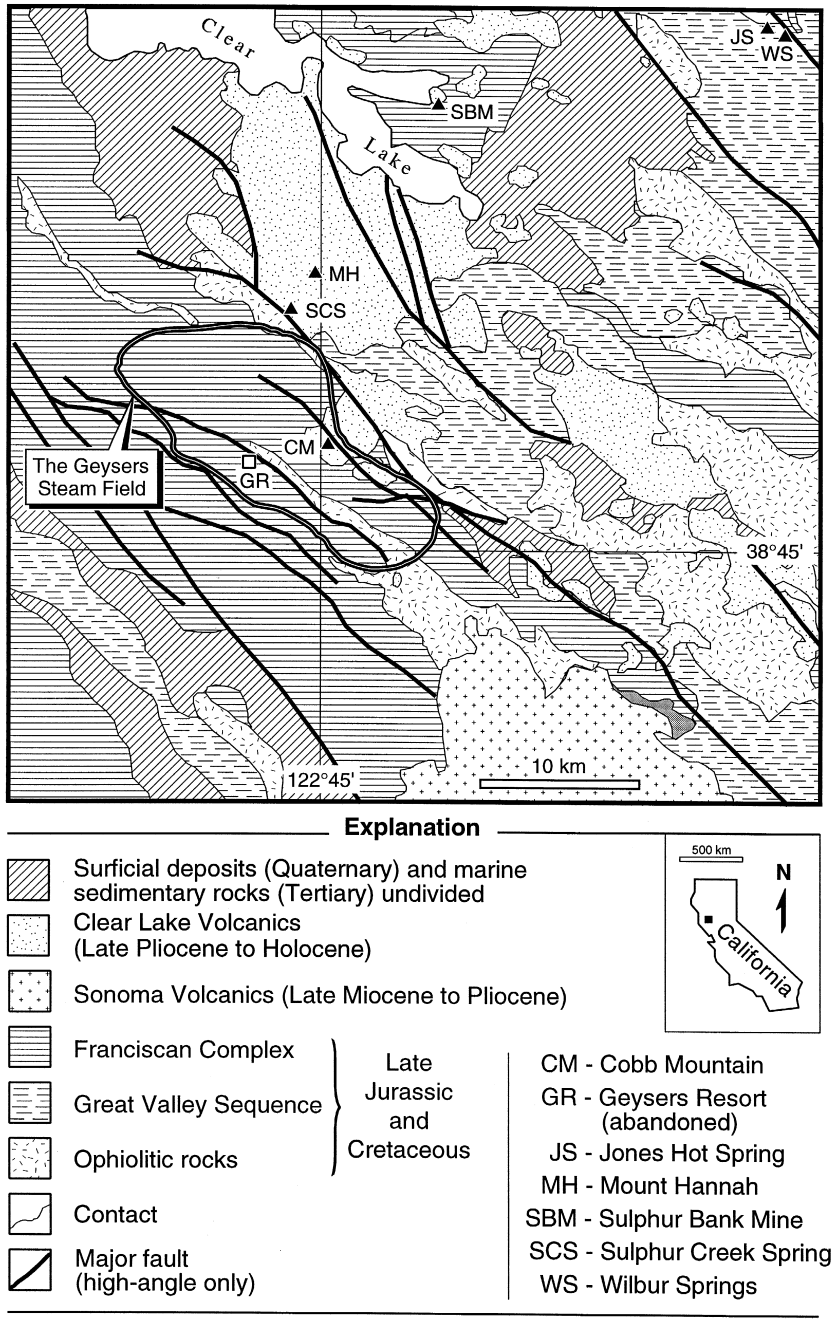

Fig. 1. Map showing the major geologic features in The Geysers–Clear Lake area (from Donnelly-Nolen et al., 1993). The productive portion of The Geysers geothermal system is outlined.

faults associated with the San Andreas transform system. These high-angle structures affect both the Mesozoic basement complex and the underlying plutonic rocks and appear to form the northeast and southwest boundaries of The Geysers steam field. Faults related to the San Andreas system may also

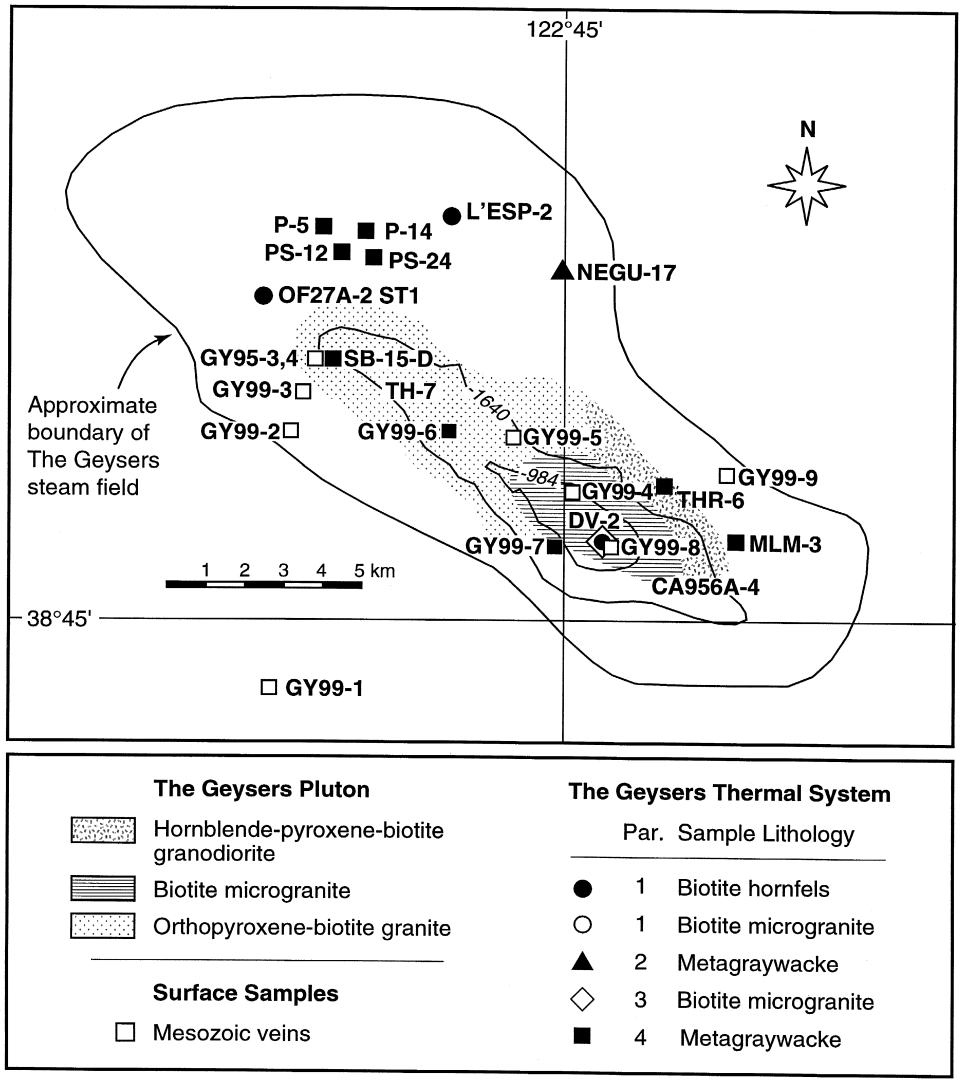

Fig. 2. Map of The Geysers showing the locations and characteristics of the well and surface vein samples discussed in the text and the distribution of intrusive phases within The Geysers pluton (modified from Hulen and Walters, 1993; Thompson, 1989). The contours (in meters relative to mean sea level) show the extent of the pluton at different elevations. The vein paragenesis (Par.) and the lithology of the host rock are indicated by symbols and discussed in the text. Parageneses 1 formed at the highest temperature, parageneses 2 to 4 represent vein formation at progressively lower temperatures. Sample numbers preceded by GY represent veins exposed at the surface or collected from the site of the Socrates retort (GY99-7). All other samples are from wells. Well abbreviations: L'ESP = L'Esperance; P = Prati; PS = Prati State; SB = Sulphur Bank; THR = Thorne.

have controlled the location of The Geysers pluton, which is centrally located within the steam field, and the distribution of the associated surficial hydrothermal alteration.

Regional metamorphism associated with subduction produced minor lawsonite, pumpellyite, glaucophane, and highly convoluted veins of quartz and carbonate (McNitt, 1968; McLaughlin, 1981; Sternfeld, 1981). Alteration related to The Geysers pluton is distinctive and easily separated from the earlier regional effects (Fig. 3). Within 600 m of the intrusive contact the metagraywacke has been altered to a

biotite hornfels containing phengite, chlorite, and biotite. Veins within the biotite hornfels contain tourmaline ± biotite ± actinolite ± clinopyroxene ± epidote + quartz + potassium feldspar or biotite ± actinolite ± clinopyroxene ± epidote + quartz + potassium feldspar (paragenesis 1). With increasing distance from the intrusion the veins are characterized by actinolite ± epidote ± ferroaxinite ± prehnite + quartz + adularia (paragenesis 2); epidote ± chlorite + quartz + adularia (paragenesis 3); and quartz + calcite ± adularia ± sericite (paragenesis 4). These hydrothermal minerals fill newly developed fractures or dissolution cavities originally occupied by calcite in the Franciscan veins (Thompson and Gunderson, 1989; Hulen et al., 1991, 1992).

Detailed investigations of paragenesis 4 in SB-15-D, Prati-5, and Prati-14 (refer to Fig. 2 for locations) demonstrate that mineralization in these wells occurred during the transition from the early liquid-dominated system to the modern vapor-dominated regime (Moore et al., 1998a). Thus, the formation of paragenesis 4 occurred much later in the cooling history of The Geysers pluton than parageneses 1 to 3, which appear to be associated with its emplacement. The majority of the gas analyses presented in this paper are of fluids trapped during the formation of this latest assemblage.

2.2. The modern vapor-dominated regime

The characteristics of vapor-dominated geothermal systems were first described by White et al. (1971) and Truesdell and White (1973). White et al. (1971) argued that vapor-dominated conditions develop when discharge exceeds recharge through the low permeability rocks surrounding the reservoir. Their model closely approximates a heat pipe in which the upward flow of steam is balanced, on a mass basis, by the downward flow of condensate (Pruess, 1985; Shook, 1995).

The modern Geysers steam field consists of two distinct, but hydraulically connected, vapor-dominated reservoirs (Drenick, 1986; Walters et al., 1988). Within the upper or normal vapor-dominated reservoir (NVDR), temperatures and pressures were close to 240°C and 35 bars before exploitation of the field began. These conditions, which remained nearly constant with depth, are close to the maximum enthalpy of saturated steam. Although White et al. (1971) assumed that a boiling water table provided the steam to the vapor-dominated reservoir, no water table has yet been encountered at The Geysers despite drilling to depths of approximately 3.9 km. It is likely that essentially all of the original liquid in the fractures has now boiled off (Truesdell et al., 1993) and that the bulk of the remaining water in the reservoir is adsorbed in microfractures and pore spaces (Ramey, 1990).

In the northern third of The Geysers, the NVDR is underlain by a region where measured temperatures range from 240°C to 342°C (Walters et al., 1988). The top of this high-temperature vapor-dominated reservoir (HTVDR) appears to be marked only by steep temperature gradients where temperatures may increase by as much as 50°C within 100 m. From heat-flow data, Williams et al. (1993) documented a 30°C to 40°C cooling within the past 5000 to 10,000 years and suggested that this event may be related to the formation of the HTVDR.

The age of the NVDR and of paragenesis 4 in the central Geysers was determined by Hulen et al. (1997) from an $^{40}Ar/^{39}Ar$ age spectrum obtained on a sample of vein adularia from SB-15-D. Several thermal models were developed that matched the spectrum. Hulen et al. (1997) favored a model yielding an abrupt temperature drop from 330°C to 240°C because fluid inclusion data demonstrated that boiling had occurred over much of this temperature interval (Moore et al., 1998a). Based on these data, it was concluded that vapor-dominated conditions developed between 0.28 and 0.25 Ma and that the system has been vapor-dominated ever since.

Steam from The Geysers is characterized by high concentrations of H_2, CH_4, CO_2, and H_2S (Table 1). The composition of the steam, however, varies both within and between the NVDR and HTVDR. Field-wide compositional variations within the NVDR reflect large-scale convection and the extent of meteoric recharge (Truesdell et al., 1987). Steam from the southeast contains the greatest proportion of recharge as indicated by δD values of -55 per mil that are similar to modern local precipitation. The corresponding $\delta^{18}O$ values of the steam (-5 to -7 per mil), however, are up to 3 per mil heavier than the local meteoric water, suggesting that it has been

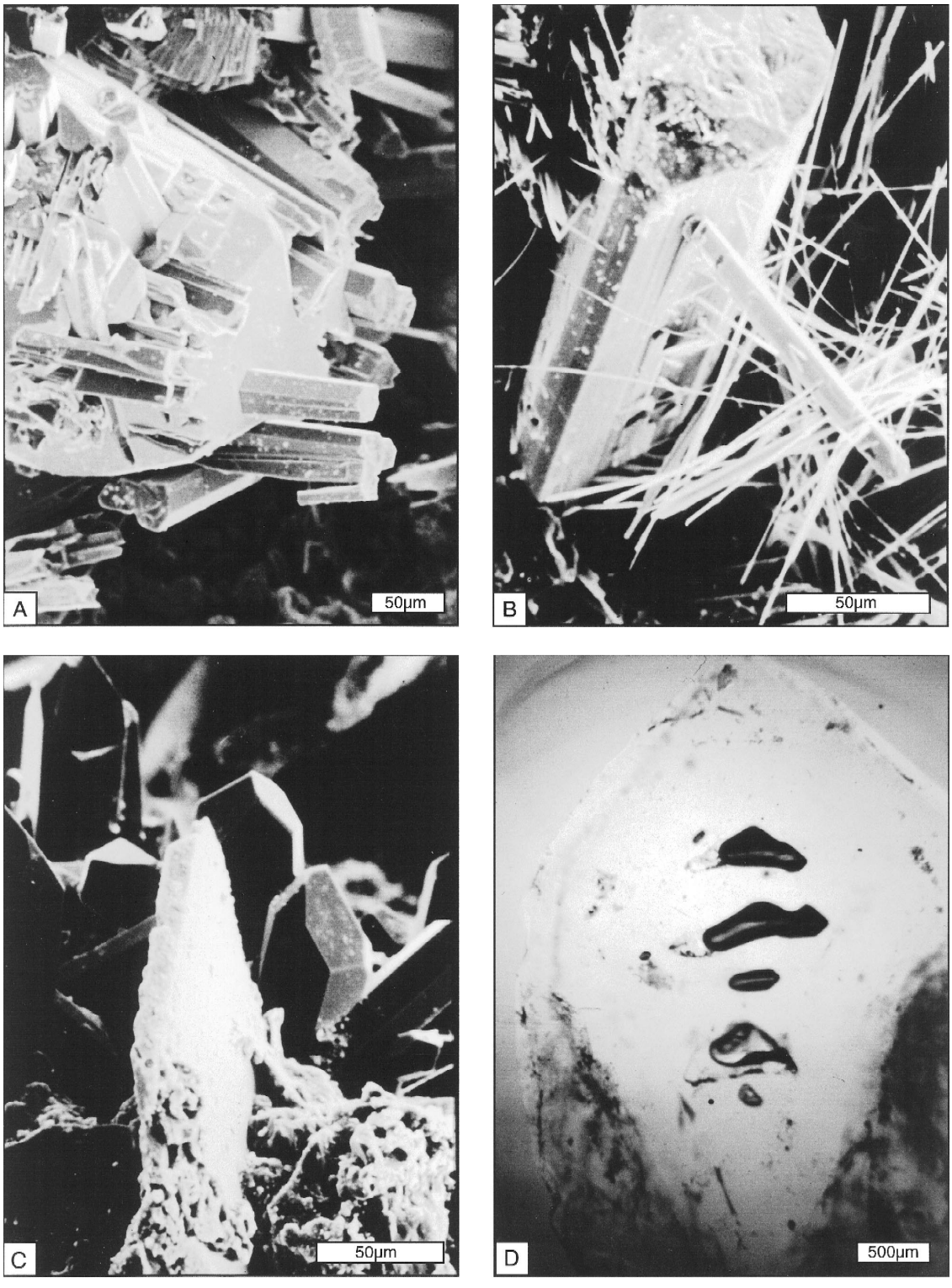
A
50μm
B
50μm
C
50μm
D
500μm

-

Table 1
Representative compositions of The Geysers steam recalculated from analyses in Truesdell et al. (1987)

	Northwest			Central			Southeast		
H_2	0.319	0.198	0.0653	0.118	0.0882	0.0151	0.0107	0.00473	0.00214
CH_4	0.299	0.113	0.018	0.0948	0.0796	0.00236	0.00483	0.000398	0.000726
H_2O	96.85	98.51	99.56	99.25	99.46	99.84	99.94	99.97	99.99
N_2	0.0372	0.0171	0.00314	0.0097	0.00866	0.00236	0.003	0.00021	0.000161
H_2S	0.0934	0.04978	0.0189	0.0347	0.0283	0.01	0.00614	0.00395	0.00193
Ar		0.000039	5.3E − 6		0.0002	0.00003	0.00005	2.0E − 6	5.6E − 7
CO_2	2.34	1.07	0.306	0.466	0.315	0.088	0.0301	0.0132	0.00389
NH_3	0.0628	0.0431	0.0267	0.0234	0.0183	0.0169	0.00317	0.00359	0.000033
N_2/Ar		438	592		43	79	60	105	288
N_2^*/Ar		991	3111		89	360	92	1003	317

Data are in mol%. N_2 from NH_3 was considered in the calculation of N_2^*/Ar.

affected by water–rock interactions. Both δD and $\delta^{18}O$ become increasingly enriched to the northwest (-40 to -50 and $+1$ to $+3$ per mil, respectively) as does the concentration of gaseous species in the steam. Steam from this part of the field is isotopically similar to the crustal waters that discharge from Mesozoic rocks at Wilber Springs and the Sulphur Bank Mine (Fig. 1; White et al., 1973; Beall, 1985; Donnelly-Nolan et al., 1993). In this paper, we use the general term crustal, rather than metamorphic, connate or evolved, to describe fluids that have a significant component of crustally derived gaseous species and dissolved solids. Although the chemistry of crustal fluids will approach equilibrium with the wall rocks, the terms metamorphic, connate or evolved imply that such fluids are old. Because we are uncertain of the age of these crustal fluids, we prefer a term based on chemistry that does not imply an age. The parent of the crustal fluids is assumed to be meteoric water, which we use for waters involved in the meteorological cycle. These fluids have total dissolved solids (TDS) of less than a few thousand parts per million and gas compositions near that of air-saturated water. However, at The Geysers, mixing of meteoric and crustal components with magmatic fluids cannot be ruled out (D'Amore and Bolognesi, 1994). Chemically, steam from the HTVDR is characterized by higher non-condensable gas, Cl (>1 ppmw), and H_2S contents, lower NH_3 contents, and enrichments in $\delta^{18}O$ compared to the NVDR (Walters et al., 1988; Haizlip and Truesdell, 1989).

2.3. Fluid inclusion characteristics of The Geysers

Fluid inclusions are common in vein quartz and calcite, and have been found in epidote and actinolite. Fig. 4 and Table 2 summarize the results of measurements on more than 1800 fluid inclusions studied by Moore and Gunderson (1995) and Moore et al. (1998a). The data were pressure corrected, where necessary, based on the elevation of the topographic surface defined by extrusive volcanic rocks that are contemporaneous with the main phases of the pluton (Donnally-Nolan et al., 1981). Maximum trapping temperatures were found to vary systematically with distance from the intrusion, ranging from approximately 440°C within the biotite hornfels at a distance of 282 m to approximately 305°C at a distance of 1730 m. The corresponding maximum

Fig. 3. Mineralogic features of the hydrothermal veins. (A) Paragenesis 1. SEM BSE image of tourmaline enclosed in adularia. (B) Paragenesis 2. SEM BSE image of fibrous actinolite and coarse-grained epidote. (C) Paragenesis 4. SEM BSE image of bladed calcite, quartz, and aggregates of late-stage clays. The clays coat the quartz and calcite. (D) Quartz crystal from SB-15-D-459.0 m (paragenesis 4). Several large primary vapor-rich inclusions trapped on rhombohedral faces are visible in the center of the crystal; secondary liquid-rich inclusions fill healed fractures on the lower outer edges. These large vapor-rich inclusions are characteristic of paragenesis 4. See text for complete assemblages.

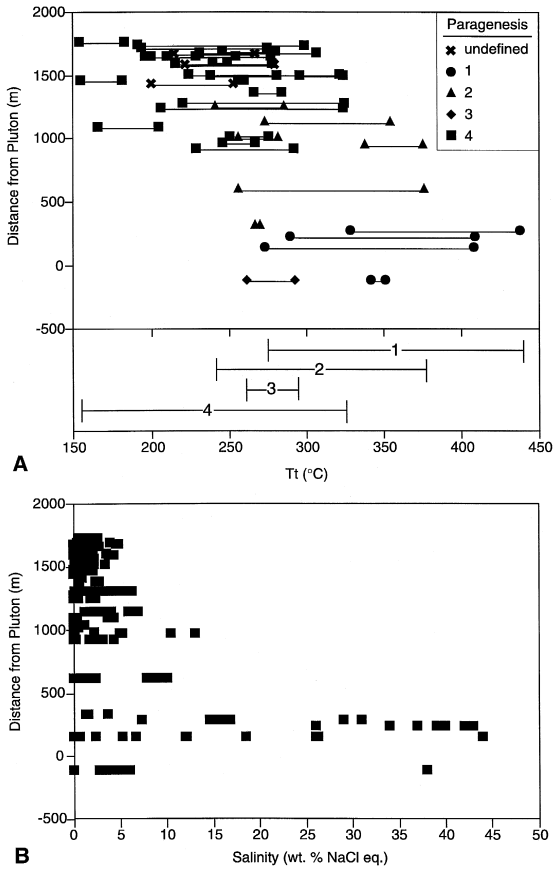

Fig. 4. Fluid inclusion trapping temperatures and salinities with respect to distance from the pluton. (A) Ranges of pressure corrected trapping temperatures (Tt (°C)) of parageneses 1 to 4. (B) Salinities of the fluid inclusions. Figures modified from Moore and Gunderson (1995).

salinities ranged from 44 to 5 wt.% NaCl equivalent. Phase relationships, combined with the field data, require lithostatic pressures during trapping of the hypersaline inclusions within the biotite hornfels and underlying pluton but are consistent with hydrostatic pressures at greater distances. While not common, the development of local overpressuring is demonstrated by the occurrence of hydrothermal breccias associated with fluid inclusion temperatures that exceed those predicted for hydrostatic pressures.

Although minor boiling occurred intermittently during the liquid-dominated stage of the hydrothermal system, the effects of boiling between 0.28 and 0.25 Ma, when the system became vapor dominated, far outweigh those of other processes. The boiling-off of the early liquids is most clearly reflected in the fluid inclusion and mineralogic characteristics of paragenesis 4 (Moore et al., 1998a). Quartz crystals deposited during this event range up to several centimeters in length and can be distinguished from earlier formed quartz by the presence of numerous primary vapor-rich inclusions (refer to Fig. 3) and intergrowths of calcite. These vapor-rich inclusions are unusually large; maximum dimensions of several hundred microns are common but inclusions greater than 1 mm in length have been observed. During freezing runs, these low-pressure vapor-rich inclusions nucleate crystals of CO_2 that sublime at temperatures below -56.6°C.

Liquid-rich inclusions trapped in quartz crystals from SB-15-D recorded systematic changes in the compositions and temperatures of the boiling fluids. Two groups of liquid-rich inclusions were recognized. Inclusion fluids representing the boiling brine indicate that the initial salinities of 1 to 2 wt.% NaCl equivalent increased to 3% to 4% during boiling and then decreased in response to mixing with low-salinity waters. The second group of fluids had nil salinities but similar temperatures and can be interpreted as representing steam condensate. Homogenization temperatures indicate that boiling was initiated in SB-15-D at approximately 300°C.

As the hydrothermal fluids boiled off, vapor-rich inclusions and condensate were trapped as secondary inclusions in earlier formed assemblages (parageneses 1–3). Vapor-rich inclusions are common in all of the samples studied, and dominate the fluid inclusion populations of many. The data of Moore and Gunderson (1995) implied that low-salinity condensate was being formed throughout the field by the time temperatures had dropped into the range of 250–265°C. The widespread distribution of these inclusions is important because it documents the development of mature vapor-dominated heat pipes within The Geysers hydrothermal system.

The temperature–salinity relationships recorded by the inclusions suggest that fluids of several different origins had been involved in the development of The Geysers hydrothermal system. Moore and Gunderson (1995) concluded that the hydrothermal fluids present during the liquid-dominated phase of the

Table 2
Summary of fluid inclusion characteristics. Numbers in parentheses indicate the number of inclusions analyzed. Abbreviations: Th (°C) = temperature of vapor bubble disappearance; Tm halite (°C) = dissolution temperature of halite; Tt (°C) = trapping temperature; Par. = paragenesis; und. = undefined. Salinities are in wt.% NaCl equivalent. Trapping pressures and temperatures are from Moore and Gunderson (1995) and Moore et al. (1998a)

Well	Two-phase inclusions		Three-phase inclusions			Measured depth (m)	Trapping pressure (bars)	Distance from pluton	Tt (°C)	Par.
	Th (°C)	Salinity	Th (°C)	Tm halite (°C)	Salinity					
CA956A-4	197–252 (20)	0.0–0.4 (9)				630.9	56	1443	200–253	und.
DV-2	320–330 (2)	1.4–1.7 (2)				1131.7	305	−111	342–351	1
			320 (1)	299 (1)	38 (1)	1131.7	305	−111	340	1
	257–296 (52)	0.0–6.0 (36)				1131.7	113	−111	262–300	3
L'Esperance-2	269–373 (26)	7.3–16.7 (6)				3370.8	904	282	330–441	1
			319–333 (2)	142–180 (2)	29–31 (2)	3370.8	904	282	375–385	1
MLM-3	211–320 (82)	0.2–6.3 (87)				1319.8	159	1306	220–325	4
NEGU-17	257–340 (29)	1.2–6.9 (15)				2600.2	250	1145	273–354	2
OF27A-2 ST1	238–343 (87)					3162.9	835	236	290–409	1
			238–308 (7)	297–358 (7)	38–43 (7)	3162.9	835	236	320–325[a]	1
			308 (1)	237 (1)	34 (1)	3162.9	835	236	355	1
Prati State-12	239–263 (32)	0.0–1.2 (13)				1908.0	201	1039	251–276	4
Prati State-24	238–273 (11)					1214.6	136	1699	246–280	4
Prati State-24	187–268 (65)	0.5–2.6 (68)				1243.6	133	1729	194–275	4
Prati-5	188–233 (109)	0.0–2.7 (95)				1271.0	30[b]	1655	188–233	4
SB-15-D	199–276 (64)	0.0–2.6 (31)				315.1	60[b]	1703	199–276	4
SB-15-D	208–266 (67)	0.0–0.7 (47)				346.2	52[b]	1672	208–266	4
SB-15-D	238–250 (33)	0.0–0.7 (18)				417.6	40[b]	1600	238–250	4
SB-15-D	240-283 (74)	0.0–3.7 (32)				429.8	67[b]	1588	240–283	4
SB-15-D	222-289 (175)	0.0–0.5 (99)				459.0	73[b]	1559	222–289	4
SB-15-D	227–290 (101)	0.0–0.5 (54)				471.8	74[b]	1546	227–290	4
TH-7	212–276 (34)	0.0–3.6 (19)				304.8	71	1598	216–278	4
Thorne-6	157–195 (52)	0.0–4.3 (40)				1655.1	180	1097	166–205	4
Thorne-6	148–252 (93)	0.0–2.1 (68)				1252.7	144	1466	155–260	4
Thorne-6	173–248 (56)	0.0–0.7 (40)				1225.3	141	1474	181–256	4
Thorne-6	147–175 (47)	0.0 (18)				1200.9	139	1777	154–183	4

[a] Values of Tm halite exceeding 326°C imply pressures in excess of 1 kb. No pressure-corrected temperatures are shown for these inclusions.

[b] Saturation pressure for maximum temperature. See Moore et al. (1998a) for evidence of boiling. No pressure corrections have been applied to the homogenization temperatures of the inclusions from Prati-5 or SB-15-D.

system's evolution were mainly crustal waters with initial salinities between 3 and 6 wt.% NaCl equivalent but that the early alteration of the biotite hornfels and plutonic rocks had been caused by magmatic fluids with salinities greater than 15 wt.% NaCl equivalent. The lowest-salinity, lowest-temperature fluids (less than 200–240°) trapped in the hydrothermal minerals were ascribed a meteoric origin. However, the data implied that meteoric waters were a minor component of the hydrothermal fluids.

In summary, the fluid inclusion and mineralogic data document the evolution of a hydrothermal system dominated by crustal waters and driven by a large hypabyssal intrusion. Although there is evidence of magmatic and meteoric contributions to the hydrothermal fluids, it is apparent that other chemical data are needed to establish their importance and distribution. In the following sections, we use the volatile compositions of the fluid inclusions to trace their origins. These data are then combined with the ages of the hydrothermal minerals and the compositions of the modern steam to constrain the character of the fluids that circulated through the system at different times.

2.4. Sample selection, distribution, and characteristics

Broad spectrum fluid inclusion gas analyses were performed on splits of veins obtained from surface exposures and a widely distributed set of wells (refer to Fig. 2). Vein samples from the wells had previously been characterized by Moore and Gunderson (1995) and Moore et al. (1998a). These samples are representative of all mineral parageneses and modern environments related to The Geysers hydrothermal system. A summary of the fluid inclusion measurements obtained on these samples and estimated trapping temperatures and pressures are presented in Table 2.

Despite the large number of wells that were drilled, little coring has been done at The Geysers and most of the cored intervals are relatively short. Nevertheless, emphasis was placed on the core samples because of the importance in documenting paragenetic relationships among the vein minerals. Three samples of paragenesis 1 were included in this study. Vein samples from L'Esperance-2-3370.8 m and OF27A-2 ST1-3162.9 m cut biotite hornfels within portions of the modern HTVDR where temperatures range from approximately 275°C to 300°C. The veins in OF27A-2 ST1-3162.9 m contain abundant tourmaline, biotite, actinolite, quartz, and potassium feldspar. The associated wall rocks are sulphide-rich, with up to several percent pyrite and chalcopyrite. Veins in L'Esperance-2-3370.8 m lack tourmaline but contain chlorite after biotite and actinolite, epidote, quartz, and potassium feldspar. The third sample of paragenesis 1 was recovered from biotite–microgranite in DV-2-1131.7 m and also contains tourmaline and abundant quartz. However, this sample is from the modern NVDR where temperatures are close to 240°C. Quartz from all three samples of paragenesis 1 contains hypersaline inclusions, indicating a magmatic origin.

Samples of paragenesis 2 and 3 were also obtained from the modern NVDR. Veins in NEGU-17-2600.2 m (paragenesis 2) cut metagraywacke and contain actinolite, ferroaxinite, epidote, and quartz. Paragenesis 3 is represented by quartz + epidote veins that cross cut the tourmaline veins in DV-2-1131.7 m. Samples of paragenesis 4 were recovered from both the cap rock and the top of the NVDR. These veins occur in metagraywacke throughout the field and contain quartz, calcite, and sericite.

SB-15-D, which is located in the central part of the field, was the only well deepened specifically for the purpose of obtaining core from the steam reservoir (Hulen et al., 1995). This well provided nearly 237 m of continuous core and intersected numerous intervals of coarse-grained vein quartz and bladed calcite characteristic of paragenesis 4. Because the mineralization in this well provides the most complete record of the transition from the liquid- to vapor-dominated regime, it was studied in the greatest detail.

Examples of paragenesis 4 deposited in the uppermost part of the hydrothermal system were collected from a road cut at GY99-6, and from the site of the Socrates retort (GY99-7). Vein samples from site GY99-6 contain euhedral crystals of quartz, chalcedony and traces of carbonate. This assemblage suggests that mineralization occurred at temperatures of 150°C to 200°C (Fournier, 1985). Samples of quartz veins collected from site GY99-7 appear to be typical of those associated with Hg deposits found

throughout the Clear Lake–Geysers area (Bailey, 1946; Yates and Hilpert, 1946). Many of these occurrences (including the Socrates mine) are concentrated near the southwestern margin of The Geysers steam field suggesting a genetic relationship with the underlying Geysers pluton (Walters et al., 1988; Hulen and Walters, 1993). A detailed discussion of the characteristics of the Hg mineralization and the associated hydrocarbon occurrences is given by Peabody and Einaudi (1992).

Samples of Mesozoic veins were collected from outcrops within The Geysers and in the surrounding area (refer to Fig. 2) and analyzed to establish background gas compositions. These veins were deformed during regional metamorphism of the Franciscan Complex and are filled with quartz and/or carbonate. Previous whole-rock oxygen isotope studies of Mesozoic veins in near-surface rocks indicated that they had not been affected by The Geysers thermal system (Lambert and Epstein, 1992; Moore and Gunderson, 1995). Thus, it was thought that they could be used to establish the compositions of crustal fluids formed as a result of high pressure and low- to moderate-temperature water–rock interactions.

Splits of six samples were chosen for noble gas analyses. These samples were selected to determine the distribution of magmatic gas within the hydrothermal system and the origins of the high N_2/Ar ratios found in some inclusion fluids. All three samples of paragenesis 1 were analyzed. In addition, three samples of paragenesis 4, two from SB-15-D (459.0 and 459.2 m), and one from Thorne-6-1200.9 m were studied. These samples represent different environments within the outmost portion of the thermal aureole surrounding The Geysers pluton. Fluid inclusion measurements on quartz from SB-15-D indicate that mineral deposition was related to mixtures of boiling crustal and meteoric fluids. In contrast, data from Thorne-6-1200.9 m suggest that only low-temperature meteoric waters were involved in the mineralization.

3. Analytical methods

Analyses of the major and minor volatile species, including H_2O, CO_2, CH_4, H_2S, H_2, N_2, Ar, and C_{2-7} organic species were performed on bulk vein samples and on individual crystals. Because of their fine grain size, only bulk analyses of parageneses 1 and 2, and the older Mesozoic veins were possible. Analyses of samples of parageneses 3 and 4 were conducted on individual crystals of quartz or calcite to simplify interpretation of the data. The gases were analyzed with a Balzers QMS 420 quadrupole mass spectrometer after being released from the inclusions by either thermal decrepitation or crushing. Details of the analytical techniques are described by Norman and Sawkins (1987) and Norman et al. (1996).

Both methods of releasing the volatiles have advantages and limitations. Because thermal decrepitation is followed by cryogenic separation of the volatiles into liquid N_2 non-condensable, liquid N_2 condensable, and aqueous fractions (thermal decrepitation–cryogenic separation, TDCS method), this method provides the greatest precision and allows for the analysis of the largest number of species. A liquid N_2 cooled charcoal trap is used to separate active non-condensable species from rare gas species. The quantity of each fraction is determined by pressure measurement in a known volume. Analytical precision is 5% or better for most species. Sample size is typically 2 g, but quantities as small as 50 mg can be analyzed. A bake-out period of 1 day was used while heating to 125°C to 200°C. However, the fluid inclusions must be heated above their homogenization temperatures (typically 400°C to 500°C) before they will decrepitate. There is evidence that the inclusion gaseous species reequilibrate to the furnace temperatures during heating (Norman and Sawkins, 1987; Norman et al. 1991). The concentrations of H_2, CO_2, and CH_4 at the time they were trapped were estimated by assuming an equilibrium assemblage of species at the average fluid inclusion trapping temperature (Norman et al., 1991).

Crushing involves opening inclusions with a swift crush in a vacuum chamber housing the mass spectrometer. The volatiles are removed by the vacuum pumping system in 1 or 2 s and recorded by operating the quadrupole in a fast scan mode with measurements taken every 150 to 200 ms (crush-fast scan; CFS method). Crushing measures far fewer inclusions than does decrepitation. Opening a 10 to 20 μm inclusion or group of smaller inclusions of equivalent volume provides the ideal amount of

Table 3
Representative TDCS and CFS analyses of fluid inclusions in bulk vein samples (parageneses 1, 2, and Mesozoic veins) and individual quartz crystals (parageneses 3 and 4). All analyses are in mol%. Abbreviations: HTVDR = high-temperature vapor-dominated reservoir; NVDR = normal vapor-dominated reservoir; n.d. = not detected; n.a. = not analyzed; Tt (°C) = average trapping temperature used to correct the TDCS analyses. See text for a discussion of the mineral parageneses and Fig. 1 for abbreviations of well names

Well	L'Esp-2	OF27A-2 ST1	DV-2	DV-2	DV-2	NEGU-17	DV-2	DV-2
Depth (m)	3370.8	3162.9	1131.7	1131.7	1131.7	2600.2	1131.7	1131.7
Paragenesis	1 (HTVDR)	1 (HTVDR)	1 (NVDR)	1 (NVDR)	1 (NVDR)	2 (NVDR)	3 (NVDR)	3 (NVDR)
H_2	0.485	0.371	0.348	2.846	0.759	0.182	7.645	2.937
He	0.00001	0.00001	0.00206	0.00460	0.00246	0.00001	0.00073	0.00126
CH_4	1.17	0.98	1.25	4.65	0.17	1.36	8.81	1.57
H_2O	88.2	92.6	83.0	91.4	98.2	95.3	67.1	95.1
N_2	0.102	0.232	0.436	0.640	0.570	0.099	n.d.	0.147
H_2S	n.d.	0.280	0.005	n.d.	n.d.	0.001	0.136	0.001
Ar	0.00004	0.00010	0.00821	0.00405	0.01195	0.00004	0.00794	0.00236
C_nH_n				0.067	0.010			0.006
CO_2	8.75	4.33	13.71	0.40	0.24	2.53	14.96	0.23
SO_2	0.045	0.001	0.001	n.d.	n.d.	0.004	0.011	0.001
C_2H_4	0.124	0.113	0.135	n.a.	n.a.	0.000	0.404	n.a.
C_2H_6	0.326	0.218	0.435	n.a.	n.a.	0.094	0.481	n.a.
C_3H_6	0.194	0.104	0.059	n.a.	n.a.	0.017	0.187	n.a.
C_3H_8	0.456	0.085	0.147	n.a.	n.a.	0.089	0.190	n.a.
C_4H_8	0.031	0.001	0.019	n.a.	n.a.	0.008	0.036	n.a.
C_4H_{10}	n.d.	n.d.	0.003	n.a.	n.a.	0.001	0.006	n.a.
C_5H_{10}	0.021	n.d.	0.011	n.a.	n.a.	0.006	0.016	n.a.
C_6H_6	n.d.	n.d.	0.001	n.a.	n.a.	0.001	0.001	n.a.
C_7H_8	n.d.	n.d.	n.d.	n.a.	n.a.	n.d.	n.d.	n.a.
N_2/Ar	2550	2320	53	158	48	2475		62
Tt (°C)	385	337	347			314	281	
Method	TDCS	TDCS	TDCS	CFS	CFS	TDCS	TDCS	CFS

Well	Prati-5	SB-15-D	SB-15-D	SB-15-D	SB-15-D	MLM-3	GY95-3	GY95-4
Depth (m)	1271.0	459.0	459.0	471.8	471.8	1319.8	Surface	Surface
Paragenesis	4 (cap rock)	4 (NVDR)	4 (NVDR)	4 (NVDR)	4 (NVDR)	4 (cap rock)	Mesozoic vein	Mesozoic vein
H_2	1.651	0.172	0.020	0.037	0.225	0.968	0.022	n.d.
He	n.d.	0.00603	0.00117	0.00002	0.03598	0.01163	0.00111	0.02859
CH_4	8.32	6.43	0.11	1.19	0.43	0.31	1.00	1.04
H_2O	37.0	80.0	99.6	79.3	98.2	85.5	98.6	98.7
N_2	2.250	0.517	0.025	0.888	0.044	0.137	0.257	0.147
H_2S	0.028	0.004	0.001	n.d.	0.002	n.d.	n.d.	0.016
Ar	0.00296	0.00116	0.00010	0.00172	0.00099	0.00287	0.00125	0.00047
C_nH_n	0.046		0.001		0.004		0.002	0.010
CO_2	50.63	12.14	0.25	17.68	1.06	12.52	0.06	0.04
SO_2	0.002	n.d.	n.d.	0.001	0.001	0.007	n.d.	0.002
C_2H_4	n.a.	n.d.	n.a.	n.d.	n.a.	n.d.	n.a.	n.a.
C_2H_6	n.a.	0.372	n.a.	0.254	n.a.	0.214	n.a.	n.a.
C_3H_6	n.a.	0.040	n.a.	0.158	n.a.	0.047	n.a.	n.a.
C_3H_8	n.a.	0.055	n.a.	0.129	n.a.	0.305	n.a.	n.a.
C_4H_8	n.a.	0.007	n.a.	0.210	n.a.	0.012	n.a.	n.a.
C_4H_{10}	n.a.	0.001	n.a.	0.049	n.a.	0.001	n.a.	n.a.
C_5H_{10}	n.a.	0.002	n.a.	0.066	n.a.	0.007	n.a.	n.a.

Table 3 (*continued*)

Well	Prati-5	SB-15-D	SB-15-D	SB-15-D	SB-15-D	MLM-3	GY95-3	GY95-4
Depth (m)	1271.0	459.0	459.0	471.8	471.8	1319.8	Surface	Surface
Paragenesis	4 (cap rock)	4 (NVDR)	4 (NVDR)	4 (NVDR)	4 (NVDR)	4 (cap rock)	Mesozoic vein	Mesozoic vein
C_6H_6	n.a.	0.000	n.a.	0.000	n.a.	n.d.	n.a.	n.a.
C_7H_8	n.a.	0.000	n.a.	0.000	n.a.	n.d.	n.a.	n.a.
N_2/Ar	759	446	263	515	45	48		
Tt (°C)		234		253		273	206	313
Method	CFS	TDCS	CFS	TDCS	CFS	TDCS	CFS	CFS

volatiles for the analysis. A 40-μm inclusion will overload the vacuum system. Five to twenty crushes are made on a 0.2 g sample with the expectation that some of the analyses will be failures.

The precision of the CFS analyses is lower than that of the TDCS method. The precision was estimated from the repeatability of the gas ratio measurements and is dependent on the size of the volatile burst that ranges from 10^8 to 10^3 counts. Precision varies from 20% for gaseous specie/water ratios and 10% for gas specie ratios for smaller bursts to 10% and 5%, respectively, for larger bursts. Bursts with counts of less than 10^5 are rejected because of poor precision.

NH_3 is rarely detected because of the interferences of secondary H_2O peaks at $m/e = 17$ and 16 and He at concentrations below 30 ppm is interfered with by the tail on the H_2 peak.

Organic compounds, principally propane (C_3H_8) and propene (C_3H_6) may interfere with the measurement of Ar. We measure $m/e = 41$ or 39 and it is assumed that peak is solely from propene because it interferes more strongly with the Ar peak at $m/e =$ 40 than does propane. The amount of Ar is calculated by first subtracting the calculated contribution to the 40 m/e peak from propene. The detection limit for Ar, or maximum Ar value, is taken as 20% of the propene $(C_3H_4)^+$ peak height. The maximum Ar value is used to constrain the minimum N_2/Ar ratios in the rare cases where there is such strong interference that data reduction indicates no detectable Ar.

Occasionally, we observe a significant O_2 peak. This is interpreted as absorbed air released from minor cracks. These analyses are rejected. Air contamination is more of a problem with minerals that break with rough surfaces such as sulphide minerals or have good cleavage like calcite and fluorite. We cannot make an "air" correction because N_2, O_2, and Ar are released in different proportions than in air, and the ratios of these species varies from crush to crush. Generally, increasing the bake-out period from 8 to 24 h reduces or eliminates the problem; the bake-out time at about 125°C is kept to a minimum to prevent diffusion of H_2 and He from the inclusions.

The noble gases were analyzed in a magnetic sector noble gas mass spectrometer after bulk vein samples (paragenesis 1) or handpicked crystals (parageneses 3 and 4) were crushed under a vacuum in a sample preparation line connected directly to the mass spectrometer. The released gas was purified by passing it over a series of metal alloy getters to remove reactive constituents (e.g., CO_2, H_2O vapor, N_2, etc.). The residual noble gas fraction was then adsorbed on activated charcoal cooled to 27°K. The noble gases were released separately by heating the charcoal to a pre-determined temperature and then admitted to the mass spectrometer. The abundances of He, Ne, and Ar isotopes in each sample were determined. Aliquots of air were used as calibration standards for the isotopic and elemental analyses. A procedural blank (gas processed without crushing) was analyzed prior to each sample. The blank amounts were: $^4He = (2.3–9.0) \times 10^{-11}$ cm^3 STP ($^3He = 0.7–3.0$ cm^3 STP), $^{22}Ne = (3.2–4.9) \times 10^{-12}$ cm^3 STP, and $^{36}Ar = (0.6–1.3) \times 10^{-10}$ cm^3 STP. The isotopic compositions of the Ne and Ar in the blanks were atmospheric within error and, therefore, a blank correction was applied to the measured gas amounts but not to the sample isotopic data. The He blanks consistently have ^3He in excess of ^4He rela-

tive to atmospheric composition ($^3He/^4He$ about 23 Ra) and the sample He compositions have been corrected accordingly.

4. Results

Two hundred and thirty eight CFS and TDCS analyses were performed on the samples to determine their major, minor and organic gas compositions. Representative analyses are presented in Table 3. The TDCS analyses were corrected for the average fluid inclusion trapping temperatures reported by Moore and Gunderson (1995) and Moore et al. (1998a). With the exception of quartz from Prati-5-1271.0 m, the principal component of the fluid inclusions was H_2O, which ranged from 67.1 to more than 99 mol%. CO_2 and CH_4 made up the bulk of the remaining gaseous species in these samples. CFS analyses yielded concentrations of CO_2 that ranged from 2.4×10^{-4} to 11.46 mol% whereas CH_4 ranged from 6.2×10^{-5} to 14.91 mol%. Quartz from Prati-5-1271.0 m contains numerous large vapor-rich inclusions and strong enrichments in non-condensable gaseous species indicate that these inclusions dominate in some of the CFS analyses (Tables 3 and 4). H_2O contents of inclusions in this sample ranged from 20.2 to 86.3 mol%, CO_2 from 8.31 to 50.63 mol%, and CH_4 from 2.6 to 32.67 mol%.

Hydrocarbon compounds other than CH_4 are present in most of the samples analyzed from The Geysers but only in trace amounts, and they typically comprise less than 1.5 mol% of the gaseous species. Data were obtained on the light hydrocarbons ranging from ethylene (C_2H_4) to toluene (C_7H_8). The abundances of the hydrocarbons are variable, although in most TDCS analyses ethane (C_2H_6), propene (C_3H_6), and propane (C_3H_8) dominate. The behavior of these organic compounds is not yet well understood. However, organic material is common in the altered metagraywackes and argillites and it is likely that the hydrocarbons were locally derived during the thermal maturation of this material.

Comparison of the CFS and TDCS analyses (Table 3) shows that thermal decrepitation (TDCS analyses) generally yielded higher liquid N_2 non-condensable gas contents than the majority of the CFS analyses of the same samples, although this is not universally true. Thus, the TDCS analyses must contain a higher percentage of gas from vapor-rich inclusions than the CFS analyses. This result was unexpected because liquid-rich inclusions follow steeper isochores and generate higher internal pressures than vapor-rich inclusions during heating. Consequently, gaseous components from liquid-rich inclusions are more likely to dominate the TDCS analyses.

There are several reasons why the two methods sampled different populations of fluid inclusions. First, crushing appears to have favored the rupture of liquid-rich inclusions over the isolated primary vapor-rich inclusions. This is especially true of quartz

Table 4
CFS analyses of quartz from Prati-5-1271.0 m, in mol%. Runs 5731A-E represent sequential crushes of the same crystal. Note that the N_2/Ar ratios of runs 5371D, E, and 5434D are minimum values

	5371A	5371B	5371C	5371D	5371E	5434D
H_2	0.345	1.651	2.213	0.702	3.277	3.283
CH_4	2.60	8.32	5.66	6.42	14.16	32.67
H_20	86.3	37.0	26.0	84.0	40.6	20.2
N_2	0.618	2.250	18.032	0.553	7.726	1.432
H_2S	0.004	0.028	0.036	0.003	0.008	0.000
Ar	< 0.00001	0.00296	0.00395	0.00090	0.00265	0.00221
C_nH_n	0.016	0.046	0.110	0.037	0.110	0.092
CO_2	10.04	50.63	47.67	8.31	34.02	42.16
SO_2	0.005	0.002	0.002	0.000	0.003	0.009
N_2/Ar		759	4565	615	2913	648
QA flag			1	2	2, 3	2

QA flags: (1) CO_2 off scale, minimum value reported. (2) Maximum argon. (3) CH_4 off scale, minimum value reported.

Table 5
Relative abundances of noble gases in samples of parageneses 1 and 4. OF27A-2 ST1-3162.9 m (a) and (b) refer to tourmaline- and quartz-rich fractions of the same vein. Amounts of ^{36}Ar and ^{4}He are reported as 10^{-9} cm^3 STP/g; those of ^{3}He as 10^{-14} cm^3 STP/g

Sample	Par.	Mass (g)	^{36}Ar	$F(^{4}He)$	$F(^{22}Ne)$	^{4}He	^{3}He (Ra)	$^{3}He/^{4}He$
L'Esperance-2-3370.8 m	1	0.2800	1.54	56.493 ± 0.104	0.824 ± 0.113	14.5	1.0	0.5
OF27A-2 ST1-3162.9 m (a)	1	0.2988	1.65	9.129 ± 0.008	0.791 ± 0.207	2.5	2.6	7.4
OF27A-2 ST1-3162.9 m (b)	1	0.1662	1.38	10.623 ± 0.016	0.870 ± 0.430	2.4	2.4	7.1
DV-2-1131.7 m	1	0.1463	3.85	0.608 ± 0.002	0.428 ± 0.172	0.4	0.6	10.7
SB-15-D-459.0 m	4	0.9846	–	–	–	0.6	0.6	7.1
SB-15-D-459.2 m	4	0.8475	2.13	3.885 ± 0.001	0.926 ± 0.116	1.4	1.5	7.7
Thorne-6-1200.9 m	4	0.0770	–	–	–	33.4	28.1	6.0

Analyses of paragenesis 1 were performed on bulk samples of the veins; analyses of paragenesis 4 are of quartz only. Par. = paragenesis. See text for definition of $F(i)$ values. F is in italics.

from paragenesis 4, which can contain growth zones and numerous healed fractures with liquid-rich inclusions in the outer portions of the crystals and a few large primary vapor-rich inclusions in the crystal interiors. Secondly, those crushes that did release large quantities of gas overwhelmed the vacuum system, precluding any data collection during these runs. In contrast, the adverse effects of vapor-rich inclusions on the vacuum system are minimized by the cryogenic separation that follows decrepitation of the samples. This gas was released as cracks, generated during decrepitation of the liquid-rich inclusions, propagated through the crystals.

The reasons for the differences in the N_2/Ar ratios between the TDCS and CFS analyses are due to the behavior of NH_3. NH_3 will break down when heated to TDCS temperatures yielding N_2 (and H_2), thus increasing the N_2/Ar ratio. The CFS analyses done at room temperature cannot detect NH_3 unless it is in concentrations approaching that of H_2O. Conversely, N_2 may react with H_2 to produce NH_3 in room temperature inclusions, lowering N_2 in the CFS analyses to concentrations below those in the trapped fluids. NH_3 in the highly reduced, H_2-rich steam may have originated through reactions with N_2 gas, or even through reactions that occurred during the collection process. Because it is not clear, which, if any, of these reactions has occurred, we have considered the effect of N_2 from NH_3 on the N_2/Ar ratios of the steam. Irrespective of these uncertainties, there is a broad similarity in the compositions of the inclusion fluids and the produced steam. Both have high amounts of H_2 and CH_4 and a broad range of N_2/Ar values, regardless of the amount of NH_3. This can be seen by comparing analyses shown in Tables 1 and 3 and in several of the plots presented in the following sections.

The results of the noble gas analyses are shown in Table 5 as concentrations and as $F(i)$ values, where $F(i)$ is the $i/^{36}Ar$ sample ratio normalized to the ratio in air. The isotopic compositions of Ne and Ar were indistinguishable from air. The similarity of the $F(^{22}Ne)$ values to air-saturated water [$F(^{22}Ne) < 1.0$)] suggests that meteoric water has had an influence on the noble gas inventory in the fluid inclusions (e.g., in DV-2-1131.7 m). $F(^{22}Ne)$ values approaching 1.0, however, imply that other processes or sources may also play a significant role, such as adsorbed air released during the crushing.

5. Discussion

5.1. Determination of fluid sources

Fluids formed in different geologic environments may be characterized by distinctive gas ratios or noble gas contents (Kennedy et al., 1985; Giggenbach, 1986, 1997; Hiyagon and Kennedy, 1992; Norman and Musgrave, 1994; Norman et al., 1996). Meteoric volatiles have N_2/Ar and $^{132}Xe/^{36}Ar$ ratios and concentrations of ^{22}Ne and ^{84}Kr between those of air and air-saturated water. Although the N_2/Ar ratios will typically range from 38 (air-saturated water at 20°C) to 84 (air), ratios between 15 to about 110 can result from boiling (Norman et al., 1997). Magmatic gas has He with R/Ra values greater than 0.1, N_2/Ar ratios exceeding 100, and

high CO_2/CH_4 ratios. The presence of N_2/Ar ratios greater than 100 are not, however, in themselves an indicator of a magmatic origin and some gaseous species commonly associated with magmatic fluids such as CO_2, H_2S, N_2, and CH_4 can be produced abiogenically from crustal rocks (Giggenbach, 1997).

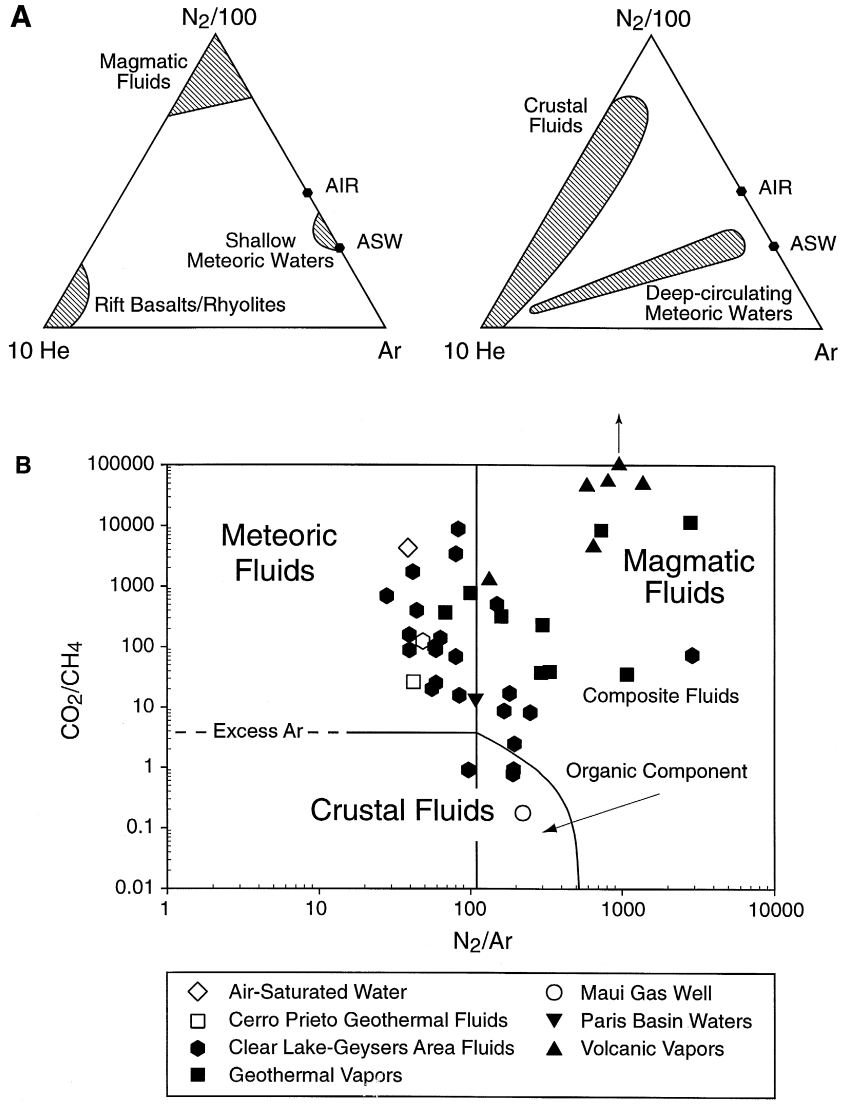

Fig. 5. Compositions of gaseous species from different geologic environments. (A) Relative He, N_2, and Ar contents of volcanic, crustal (sedimentary basin brines), and meteoric fluids, in mol% (compiled by Norman and Musgrave, 1994). The compositions of air and air-saturated water (ASW) are shown for reference. (B) CO_2/CH_4 and N_2/Ar ratios, on a molar basis, of fluids from different environments. The positions of the boundaries were taken from Norman and Moore (1999). Boiling of meteoric fluids will produce N_2/Ar ratios as low as 15 (Norman et al., 1997). Lower N_2/Ar ratios indicate loss of N_2 or the addition of Ar (area labeled Excess Ar). Degradation of plant material can produce fluids with low CO_2/CH_4 and high N_2/Ar ratios (compositional field labeled Organic Component). Composite fluids contain various proportions of gaseous species from crustal, magmatic and meteoric sources. Data sources: air-saturated water (Giggenbach and Glover, 1992); Cerro Prieto geothermal fluids (average of 1977 analyses; Nehring and D'Amore, 1984); Clear Lake–Geysers area fluids (Goff and Janik, 1993); geothermal vapors (Giggenbach, 1997); Maui gas well (Giggenbach, 1992); Paris Basin waters (average of analyses; Marty et al., 1988); volcanic vapors (Giggenbach, 1997).

Hiyagon and Kennedy (1992) found N_2/Ar ratios up to 199 in natural gas fields influenced by crustal waters. Gases of a crustal origin are identified primarily by low $^3He/^4He$ (<0.1 Ra), CO_2/CH_4 ratios less than 4, and the presence of C_{2-7} hydrocarbon compounds.

Fig. 5A, compiled by Norman and Musgrave (1994), compares the relative He, N_2, and Ar contents of gas derived from magmatic, crustal (sedimentary basins) and meteoric sources. Fig. 5B shows the compositional ranges of these fluids with respect to their CO_2/CH_4 and N_2/Ar ratios and representative analyses from different environments. We have included data on the Cerro Prieto geothermal system for comparison because it is developed in organic-rich sedimentary deposits that have some similarities to rocks in The Geysers area (Goff and Janik, 1993). Fluids that discharge from springs, gas vents and wells outside the steam field in the Clear Lake–Geysers area (Goff and Janik, 1993) are also shown in Fig. 5B. These features have temperatures up to 62°C. According to Goff and Janik (1993), only two sample sites (Sulphur Creek Spring and Wilbur Springs, see Fig. 1) yielded gas compositions similar to those of high-temperature (>200°C) geothermal systems, although $^3He/^4He$ ratios do indicate the presence of mantle derived He at most localities. These two sites had N_2/Ar ratios of 56 and 49, respectively. At the Sulphur Bank Mine (Fig. 1), where drilling has documented high temperatures (approximately 300°C) but low permeabilities (Walters et al., 1997), the N_2/Ar ratios range from 182 to 249. However, both the high temperatures and He ratios of 7.5 Ra (Goff et al., 1993) suggest the possibility that a magmatic component is present in the samples. Samples from other sites yielded N_2/Ar ratios of less than 195. The compositional relationships shown in Fig. 5B indicate that the gas compositions of the samples from the Clear Lake–Geysers area represent mixtures of crustal and meteoric components. As discussed below, our fluid inclusion gas data from this region suggest that N_2/Ar ratios greater than 525 are uniquely magmatic.

5.1.1. He–N_2–Ar relationships

Fig. 6 shows the relative He, N_2, and Ar contents of fluid inclusions determined by TDCS and CFS analyses. The data define two groups. Analyses that plot in the upper part of the ternary diagram have N_2/Ar ratios greater than about 500 and low He contents. These inclusions were found in veins that contain parageneses 1, 2, and 4. The compositions of these inclusions imply that gaseous species of a magmatic or crustal origin dominate and that irrespective of their origin, there has been little, if any, influence of meteoric fluids. The presence of a magmatic component in samples containing paragenesis 1 (L'Esperance-2-3370.8 m and OF27A-2 ST1-1131.7 m) is consistent with the occurrence of hypersaline inclusions in the vein minerals. However, there is no microscopic evidence of a magmatic influence in the samples hosting parageneses 2, 3, or 4.

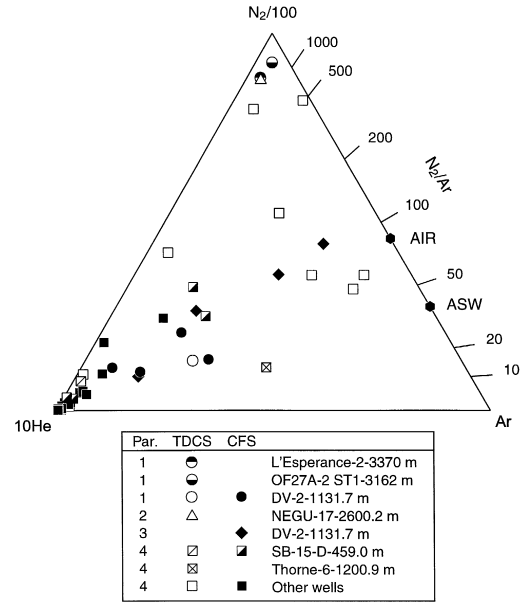

Fig. 6. Relative He, N_2, and Ar contents of fluid inclusion volatiles, in mol%. The data are grouped according to vein paragenesis (Par.) and the analytical method used (TDCS = thermal decrepitation–cryogenic separation; CFS = crush-fast scan). The compositions of air and air-saturated water (ASW) are shown on the $N_2/200$–Ar sideline. Well names are given for samples that were analyzed for their noble gases.

Veins that plot in the lower half of the ternary diagram display a much broader compositional range. Samples characterized by N_2/Ar ratios up to 110 define a trend that would be produced by the accumulation of varying amounts of He into meteoric waters. These inclusions were found in a variety of

vein types including the quartz–tourmaline vein from DV-2-1131.7 m (paragenesis 1) that also contains hypersaline inclusions, the quartz–epidote vein (paragenesis 3) from the same sample, and the veins containing paragenesis 4 from the uppermost part of the steam reservoir or modern cap rock. The occurrence of low N_2/Ar ratios in the granite-hosted quartz–tourmaline vein is significant because it suggests the influx of meteoric recharge. As discussed below, variations in the CO_2/CH_4 ratios of the inclusion fluids provide additional support for this conclusion.

N_2/Ar ratios much greater than 110 are incompatible with derivation from meteoric sources. Comparison with the inclusion fluids from the background Mesozoic veins, which generally have N_2/Ar ratios between 45 and 468 (refer to Fig. 8B), and the calculated compositions of crustal fluids shown in Fig. 5B suggest that N_2/Ar ratios up to 525 are characteristic of crustal volatiles. Thus, N_2/Ar ratios much greater than 525 are best explained as being due to the presence of a magmatic component. Inclusion analyses of paragenesis 4 that have high N_2/Ar ratios and plot near the He apex of Fig. 6 are the most significant because some of these ratios are similar to those in the upper part of the ternary diagram. Thus, their N_2 and Ar may have a similar derivation. Although the data are limited, the analyses show little evidence of mixing between fluids with high (> 500) and low N_2/Ar ratios. We infer from these relationships that the migration of He was not coupled to the flux of N_2 and Ar.

The noble gases are enriched in $^4He/^{36}Ar$ relative to meteoric water [$F(^4He) \sim 0.25$] and except for inclusions in DV-2-1131.7 m, are also enriched relative to air [$F(^4He) = 1.0$]. However, as noted above, the $F(^{22}Ne)$ values fall between the value for meteoric recharge (approximately 0.25) and air (1.0), indicating that all of the samples contain excess He. An inverse correlation between $^4He/^{36}Ar$ and the concentration of ^{36}Ar (Table 5) indicates mixing of independent components: one component is enriched in ^{36}Ar (meteoric water or air) and the other is enriched in total He with a $^3He/^4He$ ratio of 6–11 Ra or approximately 0.5 Ra, as is the case for L'Esperance-2-3370.8 m (Fig. 7). Therefore, the noble gas data require fluids that have been influenced by three independent sources: meteoric water and/or air, magmatic, and crustal.

It is noteworthy that in all of the samples except L'Esperance-2-3370.8 m, the isotopic composition of the inclusion fluids is similar to the values (6.3 to 8.3 Ra) measured in the present-day production steam (Torgersen and Jenkins, 1982; Kennedy and Truesdell, 1996). This suggests the possibility that the inclusion and reservoir fluids are in isotopic equilibrium. However, despite the similarities in their isotopic compositions and the high diffusivity of He in

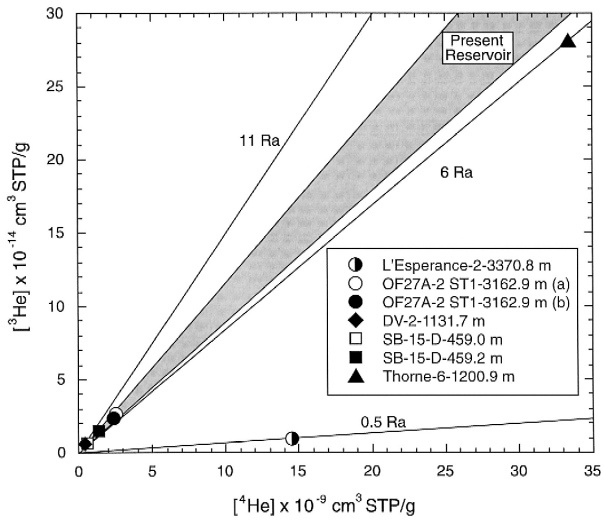

Fig. 7. Plot of ^3He vs. ^4He of the fluid inclusions and the modern steam. Refer to Table 5 for the analytical data and sample descriptions.

quartz at the present reservoir temperatures, there are several lines of evidence suggesting that the inclusion fluids record earlier conditions and that they are not in equilibrium with the fluids at depth. First, the range in the He isotopic composition of the fluid inclusions exceeds the range in the present-day fluids. Secondly, unlike the present reservoir, the fluid inclusion He isotopic composition is dependent on the position of the sample relative to the intrusion. The highest $^3He/^4He$ ratio (about 10.7 Ra) was obtained on quartz–tourmaline veins (paragenesis 1) which cut the intrusive rocks in DV-2-1131.7 m, approximately 100 m from the pluton margin. This $^3He/^4He$ ratio is significantly greater than any observed in the present reservoir. The lowest ratio (6 Ra) is from Thorne-6-1200.9 m, which was collected at the greatest distance above the intrusion (refer to Table 2). The significance of the apparent depth dependence, however, needs to be investigated further. And third, the He isotopic composition of fluid inclusions in L'Esperance-2-3370.8 m (0.5 Ra) is significantly lower than any analyzed production fluid from the present reservoir.

The very low $^3He/^4He$ ratio (0.5 Ra) in inclusions from L'Esperance-2-3370.8 m are somewhat enigmatic because the presence of hypersaline inclusions and the high N_2/Ar ratio of the sample suggested a magmatic origin. However, the low $^3He/^4He$ ratio is consistent with the high CH_4 content of this sample (Table 3) which suggests a crustal origin. Apparently, the inclusions in this sample record the influx of crustal fluids with significant concentrations of CH_4 and low $^3He/^4He$ ratios. These crustal waters may have been similar to the CH_4-rich fluids with low He isotopic compositions (1.3–1.7 Ra) that discharge from Jones Hot Spring (Fig. 1; Goff and Janik, 1993), and the CH_4-rich fluids trapped in the Mesozoic vein samples. However, our analysis of L'Esperance-2-3370.8 m has higher N_2/Ar and CO_2/CH_4 ratios. Hence, the L'Esperance-2-3370.8 m samples have been influenced by both a magmatic gas rich in CO_2 and N_2 and a CH_4- and ^4He-rich gas of crustal origin. The magmatic and crustal components have either been mixed in proportions that produced a single fluid with a reduced He isotope composition of 0.5 Ra or separate fluid inclusions enriched in magmatic and crustal gas are distributed heterogeneously within the L'Esperance-2-3370.8 m veins. These crustal fluids may have been responsible for the formation of chlorite after biotite and actinolite in this sample.

5.1.2. CO_2/CH_4 and N_2/Ar relationships

Unfortunately, He concentrations could not be determined on many of the samples analyzed by the CFS method because of interferences, and data on this species are unavailable for the representative analyses of the early steam compiled by Truesdell et al. (1987). Fig. 8, which utilizes the ratios of CO_2/CH_4 and N_2/Ar, provides an alternative approach to comparing the compositions of the fluid inclusion analyses with those of the modern steam.

Perhaps the most significant feature of Fig. 8 is the similarity between the gas ratios of the steam (Fig. 8A) and the fluid inclusions related to The Geysers thermal system (Fig. 8C–F), suggesting that both have been influenced by similar fluid sources and/or processes. Chemical and isotopic analyses of steam from the northwest Geysers (Truesdell et al.,1987) demonstrate that little infiltration of contemporary waters has occurred. Fluid inclusion gas species also indicate that the fluids trapped in secondary minerals in the northwest Geysers fluids had, as they do today, N_2/Ar ratios much greater than air-saturated water (Fig. 8D).

In contrast, δD values of the modern steam in the central and southeast Geysers clearly indicate that the reservoir fluid is dominated by meteoric water (Truesdell et al., 1987). Although this conclusion is consistent with the N_2/Ar ratios of the steam from the central Geysers and one of the analyses from the southeast, their relatively low CO_2/CH_4 ratios suggest that they also contain gaseous species derived from a crustal source (Fig. 8A). The remaining two analyses from the southeast, with higher N_2/Ar ratios, may also contain N_2 derived from a second source.

The timing of meteoric recharge into the central Geysers can be deduced from the fluid inclusion record and the results of the $^{40}Ar/^{39}Ar$ spectrum dating presented by Hulen et al. (1997). Examination of the fluid inclusion gas compositions from SB-15-D (Fig. 8E) shows that all of the TDCS analyses and most of the CFS analyses of quartz-hosted inclusions from a depth of 459.0 m have N_2/Ar ratios that fall outside the fields of crustal and meteoric fluids. In

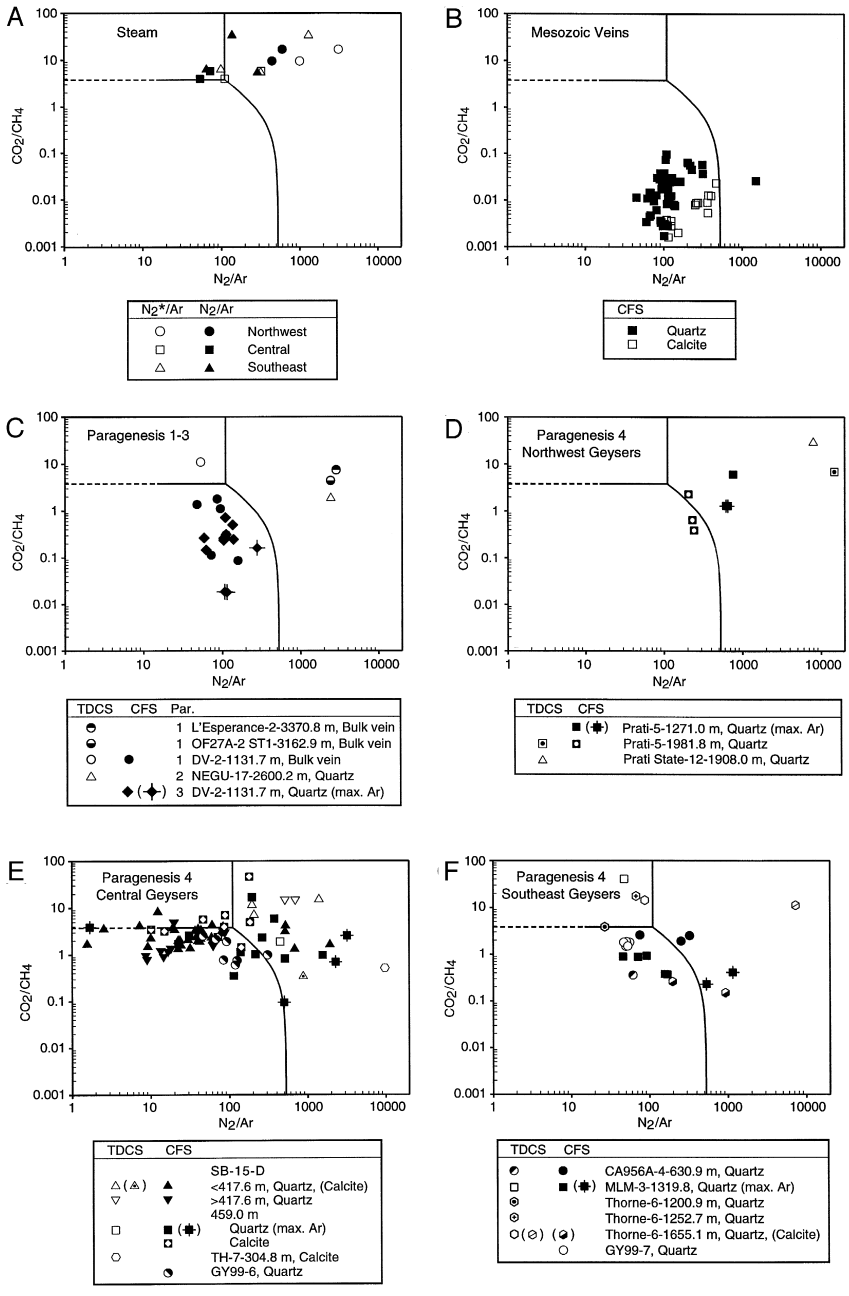

Fig. 8. CO_2/CH_4 vs.N_2/Ar ratios of fluid inclusion volatiles and the modern steam, in mol%. The boundaries of the compositional fields shown in Fig. 5 are reproduced here (see Norman and Moore, 1999 for further explanations). TDCS and CFS analyses have been distinguished for comparison. Max. Ar indicates that the Ar contents of these CFS analyses are maximum calculated values. The type of sample analyzed (bulk vein sample or individual crystal of quartz or calcite) is also shown. (A) Steam. Analyses of the steam (from Truesdell et al.,1987) are given in Table 1. Values of N_2^*/Ar (open symbols) show the effect of adding N_2 from NH_3. (B) Mesozoic veins. The veins cut metagraywacke, greenstone, and ultrabasic rocks and provide information on conditions during regional metamorphism of the Franciscan Complex. (C) Parageneses 1–3. Veins in L'Esperance-2-3370.8 m and OF27A-2 ST1-3162.9 m are from the modern high-temperature vapor-dominated reservoir; other samples are from the NVDR. (D) Paragenesis 4, northwest Geysers. (E) Paragenesis 4, central Geysers. (F) Paragenesis 4, southeast Geysers. Samples of paragenesis 4 (D–F) are from the top of the NVDR and cap rock.

contrast, the majority of CFS analyses of samples from other depths lies near the boundary between these fields and has N_2/Ar ratios less than 110. These relationships lead to the conclusion that fluids trapped early in the formation of paragenesis 4 in SB-15-D contain gaseous species derived mainly from crustal and magmatic sources whereas fluids with low N_2/Ar ratios represent the initial incursion of the meteoric waters found in this part of the field today. Like the modern steam, the CO_2/CH_4 ratios of these later fluids, which range from about 1 and 10, suggest that they accumulated gas derived from organic material in the crustal rocks. The broad range of N_2/Ar ratios to values less than air-saturated water, however, implies that boiling and other processes have modified their initial compositions. These effects are considered in the following sections.

Variations in the CO_2/CH_4 and N_2/Ar ratios of analyses from DV-2-1131.7 m (paragenesis 1 and 3, Fig. 8C) and the southeast Geysers (paragenesis 4, Fig. 8F) suggest that the inclusion fluids represent mixtures of gaseous species derived from crustal ($\pm$magmatic) and meteoric sources. The N_2/Ar ratio of the meteoric end member (about 50) is typical of surficial waters. Its presence in different parts of the field suggests that the meteoric water trapped in SB-15-D had a similar initial composition. As pointed out by Kennedy and Truesdell (1996), vapor-dominated conditions are not conducive to the trapping of fluid inclusions and therefore, the fluid inclusions are unlikely to contain any record of the modern thermal regime. Thus, the trapping of meteoric fluids in minerals from SB-15-D, which record the transition from liquid to vapor-dominated conditions, must have occurred between 0.28 and 0.25 Ma (Hulen et al., 1997). It is likely that meteoric fluids were incorporated into the hydrothermal system only during the latter part of this transitional period, when pressures were reduced and significant mixing of high- and low-salinity fluids occurred (Moore et al., 1998a).

The differences in the extent of meteoric recharge between the northwest Geysers and other parts of the field imply that permeabilities have always been highest in the southeast and central Geysers. Lower permeabilities would have inhibited meteoric recharge to the northwest. Supporting evidence for strong permeability gradients across the field is provided by whole-rock oxygen isotope data which indicate that rocks of the Franciscan Complex in the northwest are typically less isotopically exchanged than those in the central and southeast Geysers (Moore and Gunderson, 1995; Walters et al., 1996).

The distinctive chemistries of the Mesozoic surface vein samples are apparent in Fig. 8B. The most significant features of these analyses are their low CO_2/CH_4 ratios, which ranged from 0.002 to 0.1 and the limited compositional variation displayed by individual samples. This is well illustrated by the two groupings of calcite-hosted inclusions. Analyses of calcite from GY99-3 (Fig. 2) yielded N_2/Ar ratios of 254 to 468 and CO_2/CH_4 ratios of 0.005 to 0.013; those from GY99-9 ranged from 113 to 153 and 0.002 to 0.008, respectively. The CO_2/CH_4 ratios of the Mesozoic veins are up to several orders of magnitude lower than those of either the modern steam or fluids trapped in vein quartz and calcite related to The Geysers hydrothermal system. Although many of the lower N_2/Ar ratios of the Mesozoic veins are typical of meteoric waters, the range of CO_2/CH_4 ratios argues that the effects of modern meteoric infiltration on the inclusion compositions have been negligible. Similarly, there is little indication in these analyses for the presence of a magmatic component.

Analyses from SB-15-D also suggest that the CH_4 was derived from the thermal decomposition of organic debris contained in the metagraywackes and argillites. This conclusion is supported by the strong correlation ($R^2 = 0.84$ to 0.98) between log CH_4 and log C_{2-7} from seven of the eight depth intervals studied in this well. It is likely that the hydrocarbons and CH_4 trapped in the intrusive rocks in DV-2-1131.7 m (Table 3) were also derived from organic material, as the fluids circulated through the surrounding rocks.

5.1.3. H_2S–SO_2 relationships

Despite the overall similarities between the fluid inclusion and steam compositions, there are some important differences. The most significant of these are the higher proportion of H_2S relative to CO_2 and CH_4 in the produced steam (Fig. 9) and the presence of SO_2 in analyses of the inclusion fluids. High concentrations of H_2S can be explained by differences in equilibrium between H_2S in the aqueous

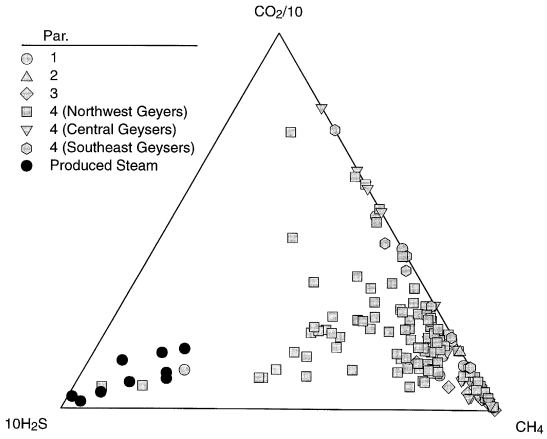

Fig. 9. Relative H_2S, CO_2, and CH_4 contents of fluid inclusions and modern steam from The Geysers, in mol%. Par. = paragenesis.

fluids and pyrite and H_2S in the vapor phase and pyrite. The activity of H_2S is much higher in an aqueous fluid at 200°C to 300°C than in the vapor. Thus, the lower relative concentrations of H_2S in the inclusions are consistent with trapping before the modern vapor-dominated conditions had become fully established.

The origin of the SO_2 is problematic. SO_2 is the dominant sulphur species in high-temperature volcanic gas (Symonds et al., 1994) and therefore, is most likely to be found in samples that contain hypersaline inclusions. Fig. 10 compares the decrepitation spectra obtained on OF27A-2 ST1-3162.9 m and L'Esperance-2-3370.8 m (see Table 3 for analyses). OF27A-2 ST1-3162.9 m contains several percent pyrite and chalcopyrite. Because both samples yielded maximum homogenization temperatures near the TDCS decrepitation temperatures, the effects of heating on the gas compositions are minimal. The presence of SO_2 in L'Esperance-2-3370.8 m is indicated by peaks at $m/e = 64$, 48, and 32. The spectrum from OF27A-2 ST1-3162 m, in contrast, has strong peaks at $m/e = 32$, 33, and 34 which are indicative of H_2S. Only trace amounts of SO_2 are present in this sample.

However, SO_2 is not expected to be stable at the lower temperatures recorded by inclusions from the outer portions of the thermal aureole. Nevertheless, trace amounts are present in many of the analyses. A compilation of fluid inclusion gas data by Graney and Kesler (1994) shows that minor SO_2 has also been reported in analyses of fluid inclusions from numerous ore deposits. Graney (1994) concluded that SO_2 could be generated by reactions between H_2S, NaCl, and H_2O released from the inclusions and O_2 contained in trace amounts of air left after the extraction line is evacuated. A more probable explanation is that the reaction between SO_2 and H_2O:

$$4SO_2 + 4H_2O = 3H_2SO_4 + H_2S \quad (1)$$

which occurs as the inclusion fluids are cooled to temperatures below about 400°C, is reversed when

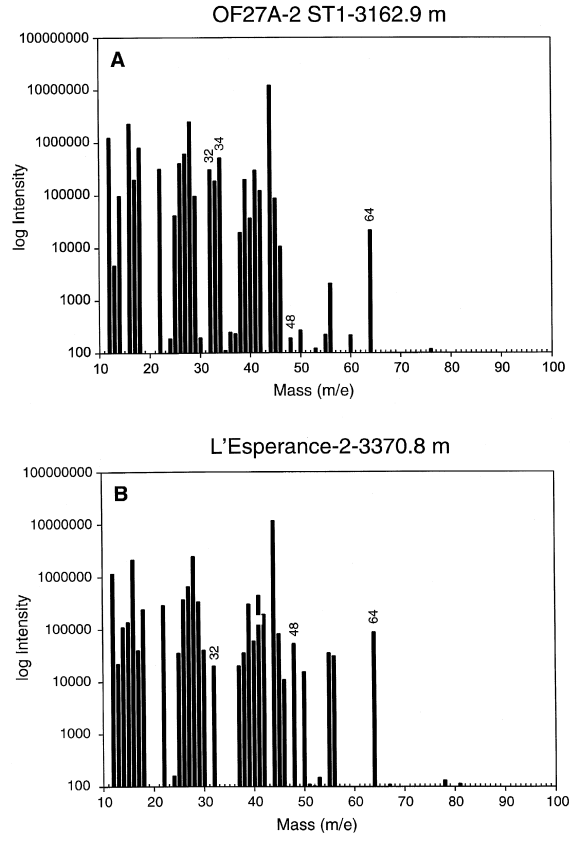

Fig. 10. Mass spectra of paragenesis 1 assemblages. Veins from both samples contain hypersaline inclusions. (A) Spectrum for OF27A-2 ST1-3162.9 m. The sample contains abundant H_2S but only minor SO_2. H_2S is identified by peaks at $m/e = 32$, 33, and 34. SO_2 gives peaks at $m/e = 64$, 48, and 32. The abundance of SO_2 is calculated from the peak at $m/e = 48$. (B) Spectrum for L'Esperance-2-3370.8 m. This sample contains abundant SO_2 but only minor H_2S.

the inclusions are opened. It is generally assumed that H^+ from the dissociation of H_2SO_4 generated by the above reaction is removed from solution by hydrolysis reactions and, hence, only limited back reaction is expected. Therefore, the presence of SO_2 may be related to the available H^+ in the inclusions. Irrespective of its origin, our data clearly indicate that SO_2 was present in some of the inclusion fluids released during analysis. Despite the low trapping temperatures of some inclusions, the He isotopic ratios demonstrate that they all contain a magmatic component.

5.2. The effects of boiling

Boiling can be recognized from fluid inclusion gas analyses by progressive changes in the composition of the coexisting liquid and vapor phases (Thomas and Spooner, 1992; Norman et al., 1997; Sawaki et al., 1997) and by gas contents that are variable and unreasonably high for the trapping pressures (Norman et al., 1996). Approximately 40% of the samples we analyzed from the modern cap rock and top of the steam reservoir (paragenesis 4), where trapping pressures and temperatures were less than 200 bars and 300°C (Moore and Gunderson, 1995) yielded gas contents that were greater than 2 mol%. Under these conditions, Henry's law coefficients predict gas contents of no more than a few mole percent in the liquid phase while concentrations of more than 1.5 mol% CO_2 in the reservoir liquid are precluded by the failure of clathrate to nucleate during freezing (Sasada, 1985). Thus, the majority of the fluid inclusion gas analyses must represent mixtures of liquid- and vapor-rich inclusions. Because the proportion of liquid- and vapor-rich inclusions will vary between sequential crushes or TDCS analyses, the analyses will generally not yield the true chemistry of either the liquid or vapor phase.

A significant exception to this generalization are the gas-rich CFS analyses from Prati-5-1271.0 m (refer to Table 4). These analyses are distinguished by extremely low H_2O and high CO_2, CH_4, H_2, and N_2 contents. Such high gas contents indicate that the inclusions must have trapped early-formed steam and that the compositional changes induced by boiling were important in triggering mineral deposition.

High CH_4 contents of fluid inclusion gas analyses appear to be a common feature of modern geothermal systems. Studies of the Tiwi (Philippines), Broadlands-Ohaaki (New Zealand) and Kirishima (Japan) geothermal systems, for example, show that the CO_2/CH_4 ratios of the modern steam exceed those in the fluid inclusions (Norman et al., 1996; Sawaki et al., 1997; Norman et al., 1998; Moore et al., 1998b). The trapping of this CH_4-rich fluid may reflect: (a) the formation of CH_4-rich waters early in the development of a geothermal system by degradation of organic material, (b) mobilization of crustal fluids in equilibrium with the wall rocks (Giggenbach, 1997), and/or (c) the trapping of the initial steam in the fluid inclusions (vapor will have a CO_2/CH_4 ratio about 1/4 of that in the liquid at temperatures of approximately 250°C).

5.2.1. CO_2–CH_4–H_2 relationships

As a result of differences in the solubilities of the volatile species, progressive boiling will lead to an increase in the CO_2 content of the residual liquid relative to CH_4 and H_2. Fig. 11A illustrates the effects of open- and closed-system boiling from 300°C to 285°C on the ratios of CO_2, CH_4, and H_2 in the vapor phase. Although boiling in geothermal systems is generally thought to occur under closed (adiabatic)-system conditions (Simmons and Browne, 1997), open-system boiling and the loss of steam from the fluids can also occur. Open-system boiling can be significant because it can produce much greater compositional changes to the fluids than closed-system boiling. Even though evidence for open-system boiling is not commonly found, its effects have been documented in fluid inclusion investigations of geothermal systems at the Valles Caldera, NM (Sasada and Goff, 1995) and Broadlands, New Zealand (Simmons and Browne, 1997).

The boiling models demonstrate that the CH_4 to H_2 ratio remains nearly constant as the steam fraction (y) increases and that only open-system boiling could produce the range of concentrations displayed by most analyses from SB-15-D and Prati-5-1271.0 m (Fig. 11B and C). The assemblages in both of these wells are representative of paragenesis 4. The CFS data from SB-15-D describe two distinct boiling trends. The dominant trend is defined by more than 40 analyses from seven depth intervals between 315.1

and 471.8 m. This trend represents the boiling of meteoric fluids (N_2/Ar ratios < 110) that are rich in CH_4. The second trend is defined by fluids trapped in quartz and calcite from 459.0 m. This trend is characterized by N_2/Ar ratios exceeding 110. As discussed above, the high N_2/Ar ratios (refer to Fig. 8) suggest that these fluids contained volatiles derived from crustal and magmatic sources. Clearly, these fluids must have boiled prior to the incursion and boiling of the meteoric recharge.

The gas analyses of inclusion fluids from Prati-5-1271.0 m also indicate a non-meteoric origin. These fluids have N_2/Ar ratios greater than 110 and CH_4/H_2 ratios that are similar to those from SB-15-D-459.0 m. However, Prati-5-1271.0 m inclusions display a much more limited range of CO_2/CH_4 ratios (Fig. 11C).

Even though the data from both wells imply boiling under open-system conditions, this process cannot by itself produce the extreme range of compositions found in SB-15-D-459.0 m quartz or account for the differences between these inclusions and those from Prati-5-1271.0 m. These differences suggest that the inclusions in SB-15-D record a change in the composition of the system that was driven by an external source of gas or fluid. For example, the addition of a CH_4-rich volatile phase with gas ratios similar to those contained in the background samples could decrease the CO_2/CH_4 ratios of the SB-15-D-459.0 m inclusions. While CH_4 could be generated by reactions between CO_2 and H_2 in the inclusions or by diffusion of H_2 through the inclusion walls, the strong linear trends displayed by the data argue against any change in the H_2 concentrations since the inclusions were trapped at temperatures ranging from 200°C to 300°C. Therefore, the quartz-hosted inclusions in SB-15-D may be recording a change in the reservoir chemistry induced by a pulse or increase in CH_4.

5.2.2. Low N_2/Ar ratios

The effect of boiling on the N_2/Ar ratio was considered by Norman et al. (1997). Because gas

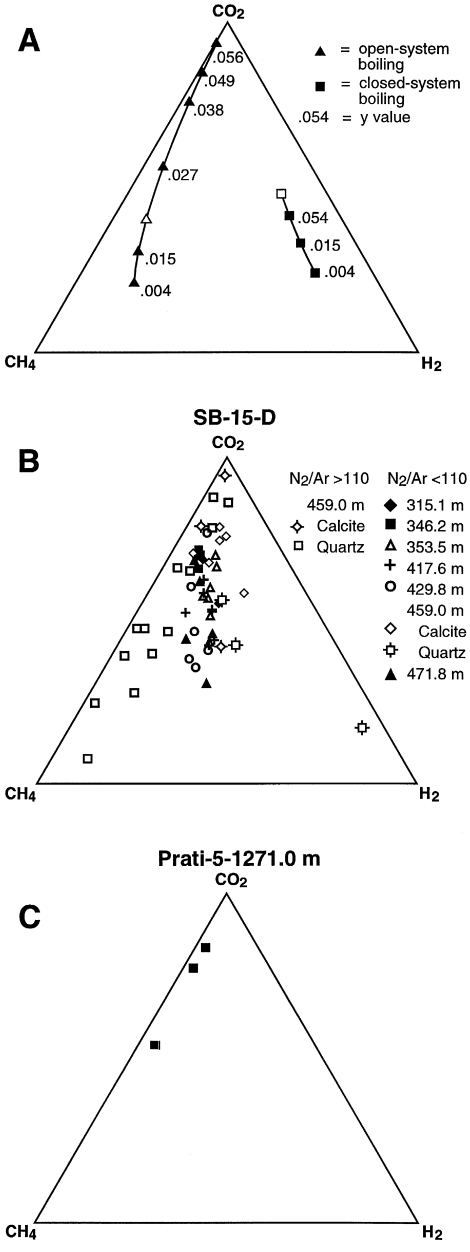

Fig. 11. The effects of boiling on CO_2, CH_4, and H_2. (A) Calculated composition of the vapor phase produced during open- and closed-system boiling between 300°C and 285°C, in mol%. The starting compositions of the fluids are shown by the open symbols. The steam fraction is given by the *y* value. Gas partitioning coefficients used in the calculation are from Giggenbach (1980). (B) The compositions of inclusion fluids from SB-15-D. Only analyses using the CFS method are shown. Sample depths are denoted by solid and open symbols. Inclusions with N_2/Ar ratios indicative of meteoric water (< 110) define a single boiling trend. A second boiling trend is defined by inclusions from SB-15-D-459.0 (quartz and calcite) with N_2/Ar ratios greater than 110. (C) Boiling trend defined by inclusions from Prati-5-1271.0 m. The inclusions have N_2/Ar ratios greater than 110.

partition coefficients for N_2 and Ar differ by a factor of approximately 2, the maximum N_2/Ar ratio of the separated vapor will be twice that of the unboiled fluid. Vapor separated from meteoric water will have a maximum N_2/Ar ratio of 110, which is slightly greater than the ratio in air (84), while the minimum N_2/Ar ratio of the boiled liquid can be as low as about 15. Lower N_2/Ar ratios of 2 to 15, which characterize some of the analyses from SB-15-D, cannot be produced by boiling of air-saturated water. Although such low N_2/Ar ratios are not common, they have been measured in active geothermal systems at Sulphur Springs, NM (Norman and Musgrave, unpublished data), and Tiwi, Philippines (Moore et al., 1998b) and in ore deposits from Mexico and Kazakhstan (Norman et al., 1997). Ratios of less than 15 require either the loss of N_2 through the formation of NH_3 complexes that are not measured, incorporation of NH_3 into secondary minerals, or the addition of radiogenic Ar from K-bearing minerals (Norman et al., 1997).

Examination of the data from SB-15-D, shown graphically in Fig. 12, indicates that the low N_2/Ar ratios are associated with decreased N_2 concentrations. Clay minerals are abundant in these samples and are a likely host for NH_3. Thus, the low N_2/Ar ratios could be due to the loss of N_2 during their formation. This possibility is strongly supported by spectral reflectance measurements on core from SB-15-D-417.6 m, which indicate the presence of ammonium illite.

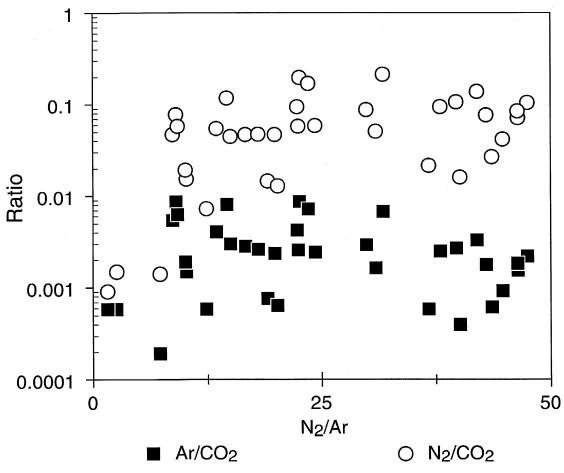

Fig. 12. Ar/CO_2 and N_2/CO_2 ratios of fluid inclusions from SB-15-D plotted against N_2/Ar. Values are in mol%. Only data obtained using the CFS technique are shown. The plot is truncated at a N_2/Ar ratio of 50 for clarity.

6. Conclusions

The Geysers is a large magmatically driven geothermal system located in northern California. Although the geothermal field produces only dry steam, petrologic observations demonstrate that the modern vapor-dominated regime evolved from a larger, liquid-dominated system (Moore and Gunderson, 1995). The initial development of this system occurred 1.2 million years ago in response to the emplacement of The Geysers pluton (Dalrymple et al., 1999). Liquid-dominated conditions persisted until 0.28 to 0.25 Ma, when the hydrothermal fluids boiled off (Hulen et al., 1997). This event is represented by intergrowths of late-stage quartz and calcite, abundant vapor-rich inclusions, and liquid-rich inclusions with low-salinities.

In this investigation, fluid inclusions representing all of the major mineral parageneses and environments within the geothermal system were systematically analyzed for H_2O, CO_2, CH_4, H_2S, H_2, N_2, Ar, and C_{2-7} and their noble gases by mass spectrometry. The data have been utilized to document the distribution of gaseous species derived from magmatic, crustal, and meteoric sources and the processes that affected them. The following conclusions can be drawn from the data.

1. The two methods used to release the major and minor inclusion gaseous species, thermal decrepitation-cryogenic separation (TDCS method) and crushing (crush-fast scan (CFS) method) resulted in the analysis of different populations of fluid inclusions. TDCS analyses typically yielded higher non-condensable gas contents than the CFS analyses indicating that the TDCS analyses contain a higher proportion of gas from vapor-rich inclusions. Although CFS analyses contain gas from both liquid and vapor-rich inclusions, liquid-rich inclusions predominate.

2. N_2/Ar and CO_2/CH_4 ratios indicate that mixtures of gaseous species derived from crustal and magmatic sources dominated the volatile compositions of the hydrothermal fluids before vapor-

dominated conditions developed. At The Geysers, the presence of a magmatic component can be identified by N_2/Ar ratios greater than 525 and high $^3He/^4He$ ratios (6–10.7 Ra). Gas derived from a crustal source is characterized by N_2/Ar ratios between 45 and 525, CO_2/CH_4 ratios less than 4, and in one sample, a He isotopic composition of 0.5 Ra.

3. Despite the high diffusivity of He, variations in its isotopic ratios demonstrate that the inclusions record conditions at the time of trapping and have not reequilibrated with the modern fluids.

4. Meteoric fluids were trapped in quartz and calcite deposited in the central and southeastern Geysers. The timing of meteoric incursion in the central Geysers is constrained by $^{40}Ar/^{39}Ar$ spectrum dating to the period when The Geysers changed from a liquid- to a vapor-dominated system (0.25–0.28 Ma; Hulen et al., 1997). Boiling modified the N_2/Ar ratios of the fluids, from ratios typical of meteoric waters (approximately 50) to values as low as 15 and as high as 110. Ratios less than 15 are occasionally observed. These low ratios are due to the incorporation of N_2 into NH_3-bearing clay minerals. No evidence of meteoric recharge was found in the gas data from the northwest Geysers. Stable isotopic compositions of the modern steam show that the circulation patterns established before vapor-dominated conditions fully developed persist today (Truesdell et al., 1987).

5. Analyses of inclusions that trapped boiling fluids can be recognized by variable gas to H_2O ratios, gas contents that are unreasonably high for the trapping temperatures and pressures, and systematic variations in their relative CH_4, CO_2, and H_2 contents. Numerical modeling of the boiling process demonstrates that boiling occurred under open-system conditions and that the inclusions have remained closed to the diffusion of H_2 since they formed.

Acknowledgements

This project could not have been undertaken without the support and encouragement of M. Reed, the Calpine Corporation, and Unocal Geothermal Operations. Our colleagues M. Adams, J. Beall, R. Fournier, J. Hulen, D. Nielson, T. Powell, G. Shook, and M. Walters generously shared their ideas with us and made numerous helpful suggestions. G. Giovani, F. Goff, H. Ross, E. Spooner, and D. Vanko reviewed an early version of the manuscript. Their comments and suggestions are greatly appreciated. Our thanks are also due to R. Person and B. Chomiak, who performed the gas analyses and to D. Jensen for drafting the figures. Funding for JNM was provided by the Office of Geothermal Technologies of the US Department of Energy under contract no. DE-AC07-95ID13274. BMK was supported by the Assistant Secretary for Energy Efficiency and Renewable Energy, Office of Geothermal Technologies of the US Department of Energy under contract no. DE-AC03-76SF00098.

References

Bailey, E.H., 1946. Quicksilver deposits of the western Mayacmas district, Sonoma County, California. Calif. Bur. Mines Rep. 42 of the State Mineralogist, pp. 200–230.

Beall, J.J., 1985. Exploration of a high temperature, fault localized, nonmeteoric geothermal system at the Sulphur Bank Mine, California. Geotherm. Resour. Counc. Trans. 9, 395–401.

Dalrymple, G.B., Grove, M., Lovera, O.M., Harrison, T.M, Hulen, J.B., Lanphere, M.A., 1999. Age and thermal history of The Geysers plutonic complex (felsite unit): Geysers geothermal field, California. Earth Planet. Sci. Lett. 173, 285–298.

D'Amore, F., Bolognesi, L., 1994. Isotopic evidence for a magmatic contribution to fluids of the geothermal systems of Larderello, Italy, and The Geysers, California. Geothermics 23, 21–32.

Donnally-Nolan, J., Hearn Jr., B.C., Curtiss, G.H., Drake, R.E., 1981. Geochronology and evolution of the Clear Lake Volcanics. In: McLaughlin, R.J., Donnelly-Nolan, J.M. (Eds.), Research in The Geysers–Clear Lake Geothermal Area, Northern California. USGS Prof. Pap. 1141, pp. 47–60.

Donnelly-Nolan, J.M., Burns, M.G., Goff, F.E., Peters, E.K., Thompson, J.M, 1993. The Geysers–Clear Lake area, California — thermal waters, mineralization, volcanism, and geothermal potential. Econ. Geol. 88, 301–316.

Drenick, A., 1986. Pressure–temperature, spinner survey in a well at The Geysers. Proc. 11th Workshop Geotherm. Reservoir Eng., Stanford Univ. pp. 197–206.

Fournier, R.O., 1985. The behavior of silica in hydrothermal solutions. In: Berger, B.R., Bethke, P.M. (Eds.), Geology and Geochemistry of Epithermal Systems. Rev. Econ. Geol. 2, pp. 45–62.

Giggenbach, W.F., 1980. Geothermal gas equilibria. Geochim. Cosmochim. Acta 44, 2021–2032.

Giggenbach, W.F., 1986. The use of gas chemistry in delineating the origin of fluid discharges over the Taupo volcanic zone: a review. Int. Volcanol. Congr., Hamilton, N. Z., Proc. Symp. 5, 47–50.

Giggenbach, W.F., 1992. Chemical techniques in geothermal exploration. In: D'Amore, F. (Ed.), Applications of Geochemistry in Geothermal Reservoir Development. United Nations Institute for Training and Research (UNITAR), pp. 119–144, E.92III.K.Man.10.

Giggenbach, W.F., 1997. The origin and evolution of fluids in magmatic–hydrothermal systems. In: Barnes, H.L. (Ed.), Geochemistry of Hydrothermal Ore Deposits. Wiley, New York, pp. 737–796.

Giggenbach, W.F., Glover, R.B., 1992. Tectonic regime and major processes governing the chemistry of water and gas discharges from the Rotorua geothermal field, New Zealand. Geothermics 21, 121–140.

Goff, F., Janik, C.J., 1993. Gas geochemistry and guide for geothermal features in the Clear Lake region, California. In: Rytuba, J.J. (Ed.), Active Geothermal Systems and Gold–Mercury Deposits in the Sonoma–Clear Lake Volcanic fields, California. Soc. Econ. Geol. Guideb. Ser. 16, pp. 207–261.

Goff, F., Kennedy, B.M., Adams, A.I, Trujillo, P.E., Counce, D., 1993. Hydrogeochemical evaluation of conventional and hot dry rock geothermal resource potential in the Clear Lake region, California. Geotherm. Resour. Counc. Trans. 17, 335–342.

Graney, J.R., 1994. Applications of mass spectrometry in economic geology and environmental geochemistry: gas composition of inclusion fluids from ore deposits and sources of lead pollution in lake sediments. PhD Thesis. Univ. Michigan, US.

Graney, J.R., Kesler, S.E., 1994. Gas composition of inclusion fluid in ore deposits: is there a relation to magmas? In: Thompson, J.F.H. (Ed.), Magmas, Fluids, and Ore Deposits. Mineral. Assoc. Can., Short Course 23, pp. 221–245.

Haizlip, J.R., Truesdell, A.H., 1989. The correlation of non-condensible gas and chloride in steam at The Geysers. Geotherm. Resour. Counc. Trans. 13, 455–460.

Hiyagon, H., Kennedy, B.M., 1992. Noble gases in CH_4-rich gas fields, Alberta, Canada. Geochim. Cosmochim. Acta 56, 1569–1589.

Hulen, J.B., Nielson, D.L., 1996. The Geysers felsite. Geotherm. Resour. Counc. Trans. 20, 298–306.

Hulen, J.B., Walters, M.A., 1993. The Geysers felsite and associated geothermal systems, alteration, mineralization, and hydrocarbon occurrences. In: Rytuba, J.J. (Ed.), Active geothermal systems and gold–mercury deposits in the Sonoma–Clear Lake volcanic fields, California. Soc. Econ. Geol. Guideb. Ser. 16, pp. 141–152.

Hulen, J.B., Walters, M.A., Nielson, D.L., 1991. Comparison of reservoir and caprock core from the Northwest Geysers steam field, California. Geotherm. Resour. Counc. Trans. 15, 11–18.

Hulen, J.B., Nielson, D.L., Martin, W., 1992. Early calcite dissolution as a major control on porosity development in The Geysers steam field, California — additional evidence from Unocal well NEGU-17. Geotherm. Resour. Counc. Trans. 16, 167–174.

Hulen, J.B, Koenig, B.A., Nielson, D.L., 1995. The Geysers coring project, Sonoma County, California USA — summary and initial results. Trans. World Geotherm. Cong., Florence, Italy, 1415–1420.

Hulen, J.B., Heizler, M.T., Stimac, J.A., Moore, J.N., Quick, J.C., 1997. New constraints on the timing of magmatism, volcanism, and the onset of vapor-dominated conditions at The Geysers steam field, California. Proc. 22nd Workshop Geotherm. Reservoir Eng., Stanford Univ. pp. 75–82.

Kennedy, B.M., Truesdell, A.H., 1996. The Northwest Geysers high-temperature reservoir: evidence for active magmatic degassing and implications for the origin of The Geysers geothermal field. Geothermics 25, 365–387.

Kennedy, B.M., Lynch, M.A., Reynolds, J.H., Smith, S.P., 1985. Intensive sampling of noble gases in fluids at Yellowstone: I. Early overview of the data; regional patterns. Geochim. Cosmochim. Acta 49, 1251–1261.

Lambert, S.J., Epstein, N.S., 1992. Stable-isotope studies of rocks and secondary minerals in a vapor-dominated hydrothermal system at The Geysers, Sonoma County, California. J. Volcanol. Geotherm. Res. 53, 199–226.

Marty, B., Criaud, A., Fouillac, C., 1988. Low enthalpy geothermal fluids from the Paris sedimentary basin: 1. Characteristics and origin of gases. Geothermics 17, 619–633.

McLaughlin, R.J., 1981. Tectonic setting of pre-Tertiary rocks and its relation to geothermal resources in The Geysers–Clear Lake area. In: McLaughlin, R.J., Donnelly-Nolan, J.M. (Eds.), Research in The Geysers–Clear Lake Geothermal Area, Northern California. USGS Prof. Pap. 1141, pp. 25–45.

McNitt, J.R., 1968. Geology of the Kelseyville quadrangle, Sonoma, Lake, and Mendocino Counties, California. Calif. Div. Mines Geol. Map Sheet 9.

Moore, J.N., Gunderson, R.P., 1995. Fluid inclusion and isotope systematics of an evolving magmatic–hydrothermal system. Geochim. Cosmochim. Acta 59, 3887–3907.

Moore, J.N., Anderson, A.J., Adams, M.C., Aines, R.D., Norman, D.I., Walters, M.A., 1998a. The fluid inclusion and mineralogic record of the transition from liquid- to vapor-dominated conditions in The Geysers geothermal system, California. Proc. 23rd Workshop Geotherm. Reservoir Eng., Stanford Univ. pp. 211–218.

Moore, J.N., Powell, T.S., Bruton, C.J., Norman, D.I., Heizler, M.T., 1998b. Thermal and chemical evolution of the Tiwi geothermal system, Philippines. Proc. 9th Int. Symp. Water–Rock Interact., Balkema, Rotterdam, pp. 671–674.

Nehring, N.L., D'Amore, F., 1984. Gas chemistry and thermometry of the Cerro Prieto, Mexico geothermal field. Geothermics 8, 75–89.

Norman, D.I., Moore, J.N., 1999. Methane and excess N_2 and Ar in geothermal fluid inclusions. Proc. 24th Workshop Geotherm. Reservoir Eng., Stanford Univ., pp. 196–202.

Norman, D.I., Musgrave, J., 1994. N_2–Ar–He compositions in fluid inclusions: indicators of fluid source. Geochim. Cosmochim. Acta 58, 1119–1131.

Norman, D.I., Sawkins, F.J., 1987. Analysis of gases in fluid inclusions by mass spectrometer. Chem. Geol. 61, 10–21.

Norman, D.I., Benton, L.D., Albinson, T.F., 1991. Calculation of fO_2 and fS_2 of ore fluids and depth and pressure of mineralization from fluid inclusion gas analyses from the Fresnillo, Colorado, and Sombrete Pb–An–Ag deposits, Mexico. Proc. SGA Anniv. Mtg: Source, Transport, and Deposition of Metals, Nancy, France. pp. 209–212.

Norman, D.I., Moore, J.N., Yonaka, B., Musgrave, J., 1996.

Gaseous species in fluid inclusions: a tracer of fluids and indicator of fluid processes. Proc. 21st Workshop Geotherm. Reservoir Eng., Stanford Univ. pp. 233–240.

Norman, D.I., Moore, J.N, Musgrave, J., 1997. Gaseous species as tracers in geothermal systems. Proc. 22nd Workshop Geotherm. Reservoir Eng., Stanford Univ. pp. 419–426.

Norman, D.I., Chomiak, B.A., Moore, J.N., 1998. Approaching equilibrium from the hot and cold sides in the FeS_2–FeS–Fe_3O_4–H_2S–CO_2–CH_4 system in light of fluid inclusion gas analysis. Proc. 9th Int. Symp. Water–Rock Interact., Balkema, Rotterdam, pp. 565–568.

Peabody, C.E., Einaudi, M.T., 1992. Origin of petroleum and mercury in the Culver-Bear cinnabar deposit, Mayacmas district, California. Econ. Geol. 87, 1078–1102.

Pruess, K., 1985. A quantitative model of vapor dominated geothermal reservoirs as heat pipes in fractured porous rocks. Geotherm. Resour. Counc. Trans. 9, 353–361.

Pulka, F.S., 1991. Subsurface geology at Ford Flat, Geysers geothermal system, California. MS Thesis. Michigan Tech. Univ., Houghton.

Ramey Jr., H.J., 1990. Adsorption in vapor-dominated systems. U. S. Dep. Energy, Proc. Geotherm. Prog. Rev. VIII, 63–67, CONF-9004131.

Sasada, M., 1985. CO_2-bearing fluid inclusions from geothermal fields. Geotherm. Resour. Counc. Trans. 9, 351–356.

Sasada, M., Goff, F., 1995. Fluid inclusion evidence for rapid formation of the vapor-dominated zone at Sulphur Springs, Valles Caldera, New Mexico, USA. J. Volcanol. Geotherm. Res. 67, 161–169.

Sawaki, T., Sasada, M., Sasaki, M., Goko, K., 1997. Fluid inclusion study of the Kirismima geothermal system, Japan. Geothermics 26, 305–327.

Shook, G.M., 1995. Development of a vapor-dominated reservoir with a "high-temperature" component. Geothermics 24, 489–505.

Simmons, S.F., Browne, P.R.L., 1997. Saline fluid inclusions in sphalerite from the Broadlands–Ohaaki geothermal system: a coincidental trapping of fluids being boiled toward dryness. Econ. Geol. 92, 485–489.

Sternfeld, J.N., 1981. The hydrothermal petrology and stable isotope geochemistry of two wells in The Geysers geothermal field, Sonoma County, California. MS Thesis. Univ. California, Riverside.

Sternfeld, J.N., 1989. Lithologic influences on fracture permeability and the distribution of steam in the Northwest Geysers steam field, Sonoma County, California. Geotherm. Resour. Counc. Trans. 13, 473–479.

Symonds, R.B., Rose, W.I., Bluth, G.J.S., Gerlach, T.M., 1994. Volcanic-gas studies: methods, results, and applications. In: Carroll, M.R., Holloway, J.R. (Eds.), Volatiles in Magmas. Rev. Mineral. 30, pp. 1–66.

Thomas, A.V., Spooner, E.T.C., 1992. The volatile geochemistry of magmatic H_2O–CO_2 fluid inclusions from the Tanco zoned granitic pegmatite, southeastern Manitoba, Canada. Geochim. Cosmochim. Acta 56, 49–65.

Thompson, R.C., 1989. Structural Stratigraphy and intrusive rocks at The Geysers geothermal field. Geotherm. Res. Counc. Trans. 13, 481–486.

Thompson, R.C., Gunderson, R.P., 1989. The orientation of steam-bearing fractures at The Geysers geothermal field. Geotherm. Resour. Counc. Trans. 13, 481–485.

Torgersen, T., Jenkins, W.J., 1982. Helium isotopes in geothermal systems: Iceland, The Geysers, Raft River, and Steamboat Springs. Geochim. Cosmochim. Acta 46, 739–748.

Truesdell, A.H., White, D.E., 1973. Production of superheated steam from vapor-dominated geothermal reservoirs. Geothermics 2, 154–173.

Truesdell, A.H., Haizlip, J.R., Box Jr., W.T., D'Amore, F., 1987. Fieldwide chemical and isotopic gradients in steam from The Geysers. Proc. 11th Workshop Geotherm. Reservoir Eng., Stanford Univ., pp. 241–246.

Truesdell, A., Walters, M., Kennedy, M., Lippmann, M., 1993. An integrated model for the origin of The Geysers geothermal field. Geotherm. Resour. Counc. Trans. 17, 273–280.

Walters, M.A., Haizlip, J.R., Sternfeld, J.N., Drenick, A.F., Combs, J., 1988. A vapor-dominated reservoir exceeding 600°F at The Geysers, Sonoma County California. Proc. 13th Workshop Geotherm. Reservoir Eng., Stanford Univ., pp. 73–81.

Walters, M.A., Moore, J.N., Nash, G.D., Renner, J.L., 1996. Oxygen isotope systematics and reservoir evolution of the Northwest Geysers, California. Geotherm. Res. Counc. Trans. 20, 413–422.

Walters, M.A., Hulen, J.B., Moore, J.N., 1997. Geology and oxygen-isotope geochemistry — Audrey A-1 geothermal well, Sulphur Bank Mine area, Lake County, California. Proc. 22nd Workshop Geotherm. Reservoir Eng., Stanford Univ., pp. 473–482.

White, D.E., Muffler, L.J.P., Truesdell, A.H., 1971. Vapor-dominated hydrothermal systems compared with hot water systems. Econ. Geol. 66, 73–81.

White, D.E., Barnes, I., O'Neil, J.R., 1973. Thermal and Mineral waters of nonmeteoric origin, California Coast Ranges. Geol. Soc. Am. Bull. 42, 547–560.

Williams, C.F., Galanis Jr., S.P., Moses Jr., T.H., Grubb, F.V., 1993. Heat-flow studies in the northwest Geysers Geothermal field, California. Geotherm. Resour. Counc. Trans. 17, 281–288.

Yates, R.G., Hilpert, L.S., 1946. Quicksilver deposits of the eastern Mayacmas district, Lake and Napa Counties, California. Calif. J. Mines Geol. 42, 231–286.